

Higher-order moment theories for dilute granular gases of smooth hard-spheres

Vinay Kumar Gupta^{1,†}, Priyanka Shukla² and Manuel Torrilhon³

¹SRM Research Institute and Department of Mathematics,
SRM University, Chennai 603203, India

²Department of Mathematics, Indian Institute of Technology Madras, Chennai 600036, India

³Center for Computational Engineering Science, Department of Mathematics,
RWTH Aachen University, Schinkelstr. 2, D-52062, Aachen, Germany

(Received xx; revised xx; accepted xx)

Grad's method of moments is employed to develop higher-order Grad's moment equations—up to first 26-moments—for granular gases within the framework of the (inelastic) Boltzmann equation. The homogeneous cooling state of a freely cooling granular gas is investigated with the Grad's 26-moment equations in a semi-linearized setting and it is shown that the granular temperature in the homogeneous cooling state still decays according to Haff's law while the other higher-order moments decay on a faster time scale. The nonlinear terms of fully contracted fourth moment are also considered and, by exploiting the stability analysis of fixed points, it is shown that these nonlinear terms have negligible effect on Haff's law. Furthermore, an even larger Grad's moment system which includes the fully contracted sixth moment is also scrutinized and the stability analysis of fixed points is again exploited to conclude that even the inclusion of scalar sixth order moment into the Grad moment system has negligible effect on Haff's law. The constitutive relations for stress and heat flux (the Navier–Stokes and Fourier relations) are obtained by performing a Chapman–Enskog-like expansion on the Grad's 26-moment equations and compared with those existing in the literature. The linear stability of the homogeneous cooling state is analyzed through the Grad's 26-moment system and various sub-systems by decomposing them into longitudinal and transverse systems. It is found that one eigenmode in both longitudinal and transverse systems in case of inelastic gases is unstable. By comparing the eigenmodes from various theories, it is established that the 13-moment eigenmode theory predicts that the unstable eigenmode remains unstable for all wavenumbers below a certain coefficient of restitution while any other higher-order moment theory shows that this mode becomes stable above some critical wavenumber for all values of coefficient of restitution. In particular, the Grad's 26-moment theory leads to a smooth profile for the critical wavenumber in contrast to the other considered theories.

1. Introduction

A conglomeration of discrete macroscopic particles characterized by dissipative collisions is termed as a granular material. Granular materials are prevalent in various industries—for instance, in chemical, agriculture and food industries—as well as in nature—for instance, in asteroid belt, sand dunes, debris, etc. Under substantially strong driving forces (e.g., vibration, shearing, etc.), granular materials are in rapid flow regime, in which they exhibit fluid-like behavior and often referred to as *granular gases* (Campbell

† Email address for correspondence: vinay.libra.gupta@gmail.com

1990; Goldhirsch 2003). In the rapid flow regime, the particles of a granular material move randomly and, similar to a molecular gas, it can be assumed that the collisions among them are binary and instantaneous. However, in contrast to a molecular gas, the collisions between any two particles of a granular material are inherently inelastic, and thereby energy is dissipated during each collision. The inelastic collisions in granular materials lead to many interesting phenomena—for instance, standing wave patterns (Melo *et al.* 1995; Umbanhowar *et al.* 1996), clustering (Kudrolli *et al.* 1997), fingering (Pouliquen *et al.* 1997), mixing and segregation (Ottino & Khakhar 2000; Mullin 2000; Breu *et al.* 2003), shear banding (Mueth *et al.* 2000; Shukla & Alam 2009), jamming (Corwin *et al.* 2005), density waves (Liss *et al.* 2002; Alam *et al.* 2009), etc. Nevertheless, the mechanics of granular material is still not well-understood, although there have been significant developments in the last couple of decades.

The analogy between granular and molecular fluids has motivated several researchers to devise theoretical methods—for studying granular fluids—based on kinetic theory within the framework of the Boltzmann equation, see e.g., Jenkins & Richman (1985*a,b*); Goldshtein & Shapiro (1995); Brey *et al.* (1996); Sela & Goldhirsch (1998); Brey *et al.* (1998); Garzó & Santos (2003); Brilliantov & Pöschel (2004); Bisi *et al.* (2004); Kremer *et al.* (2014). Kinetic theory for granular flows was first introduced in the two seminal papers by Jenkins & Savage (1983) and Lun *et al.* (1984) where the former deals with the theory for nearly elastic granular flows while the latter with arbitrary inelasticity. The reported works on the kinetic theory for granular fluids also attempted to extend the two well-known approximation methods in kinetic theory for molecular gases, namely the Chapman–Enskog expansion (CE) method (Chapman & Cowling 1970) and Grad’s method of moments (Grad 1949*b*). Despite the fact that the higher-order approximations (Burnett and beyond) resulting from CE method lead to unstable equations while the Grad’s method of moments always yields linearly stable sets of equations in case of molecular gases (Bobylev 1982), the former has extensively been studied even for granular gases. Goldshtein & Shapiro (1995) applied the CE method to obtain Euler-like hydrodynamic equations for rough granular flows. The papers by Brey *et al.* (1998) and Garzó & Dufty (1999) apply the CE method to dilute and dense granular gases, respectively, to derive the first order (Navier–Stokes and Fourier) constitutive relations for the system of mass, momentum and energy balance equations. Both the works assume that the space and time dependence of the distribution function can be expressed completely in terms of the hydrodynamic fields and represent the distribution function in a formal series of a uniformity parameter which measures the strength of spatial gradients of the hydrodynamic fields. Sela *et al.* (1996) performed a generalized expansion on the distribution function in powers of two small parameters, namely the Knudsen number and the degree of inelasticity $\epsilon = 1 - e^2$ with e being the coefficient of (normal) restitution and determined the Burnett order constitutive relations for the system of mass, momentum and energy balance equations specialized to a simply sheared two-dimensional hard-sphere granular gas via the CE method. Subsequently, with the same method, Sela & Goldhirsch (1998) (see also Gupta 2011) determined the Burnett order constitutive relations for a smooth hard-sphere granular gas in three dimensions. However, both these works restrict the coefficient of restitution for being very close to 1 in order to get the zeroth order solution in the expansion as Maxwellian, similar to a molecular gas. Lutsko (2005) employed the CE method to obtain the constitutive relations for dense granular gases with arbitrary energy loss models. His model produced the homogeneous cooling state (HCS) solution at the zeroth order in the expansion while Navier–Stokes and Fourier constitutive relations at first order. Following the approach of expanding the distribution function in powers of uniformity

parameter, Khalil *et al.* (2014) recently obtained the Burnett order constitutive relations for a smooth granular gas described with (inelastic) Maxwell interaction potential via the CE method. It is worth to point out that, unlike Sela & Goldhirsch (1998), their approach does not restrict the coefficient of restitution for being close to 1. Recently, Kremer *et al.* (2014) employed the CE method to obtain the transport coefficients up to Navier–Stokes order for a granular gas of rough hard-spheres.

Despite the success of the Grad’s method of moments over the CE method in case of molecular gases (see e.g., Torrilhon 2016, and references therein), the former in case of granular flows has received much less attention than the latter which has been investigated extensively. Nevertheless, over the last few years, researchers have shown interest in exploring the former as well (see e.g., Kremer & Marques Jr. 2011; Garzó 2013; Saha & Alam 2014). The pioneering work on Grad’s method of moments for granular flows is due to Jenkins and Richman who extended the method to granular flows and derived the Grad’s 13-moment (G13) equations for a dense and smooth granular gas in Jenkins & Richman (1985a) and, subsequently, the Grad’s 16-moment equations for a dense and rough two-dimensional granular gas in Jenkins & Richman (1985b)—the extra field variables are due to rotational motion of rough particles on collision. Bisi *et al.* (2004) further extended the Grad’s method of moments to weakly inelastic granular flows with variable coefficient of restitution, in one-dimension though. As it is well-established that the scalar fourth moment is necessary for the proper description of a granular gas, Risso & Cordero (2002) included the scalar fourth moment and—for a granular gas—obtained Grad’s moment equations for 9 hydrodynamic fields in two-dimensions (corresponding to 14 field variables in three-dimensions), and applied them to investigate two problems, namely the HCS and a granular system steadily heated by two parallel walls. Kremer & Marques Jr. (2011) presented the Grad’s 14-moment (G14) theory for dilute granular gases and by employing this theory, they investigated the HCS, found the constitutive relations for five moment equations, and performed eigenmode analysis on thirteen field theory, where they assumed a constant value for the scalar fourth moment. Garzó (2013) demonstrated the G14 theory for moderately dense granular flows, although the work aimed at finding the Navier–Stokes level constitutive relations through the G14 equations. Recently, Saha & Alam (2014) developed the Grad’s moment method based on anisotropic Gaussian and employed it to investigate the non-Newtonian stress, collisional dissipation and heat flux in a sheared two-dimensional granular flow.

The main reasons—among others—that the Grad’s method of moments for granular flows is receiving less attention could be that (i) the production terms, which emanate through the Boltzmann collision integral, in the moment equations are very difficult to evaluate for a general interaction potential, (ii) how many and which moments one should consider for describing a process is not known *a priori*, and (iii) the boundary conditions associated with the Grad’s moment equations are unclear, which is apparently also the case for higher-order equations resulting from the CE method. Over the last couple of years, the two of the present authors have developed a computational methodology, which can compute the production terms associated with the Grad’s moment equations for (i) a single molecular gas, (ii) a mixture of molecular gases and (iii) a dilute granular gas, all interacting with a general interaction potential (Gupta & Torrilhon 2012, 2015a; Gupta 2015). The *order of magnitude* method developed by Struchtrup (2004, 2005)—which regularizes the original G13 equations—identifies the required moments for describing a process in rarefied molecular gases in a systematic way, although the method requires the Grad’s 26-moment (G26) equations which at present are not available for granular gases. For the original Grad’s moment equations, it can be stated empirically that the number of moments ought to be increased with increasing rarefaction. The boundary conditions

associated with the Grad's moment equations for molecular gases are typically obtained using the Maxwell accommodation model (Maxwell 1879); however, those for granular gases are yet to be explored.

In this paper, we derive the G26 equations for dilute granular gases through the Grad's method of moments, although we neither consider the regularization of the Grad's moment equations nor the required boundary conditions—these problems will be considered elsewhere in future. The fully nonlinear production terms associated with an even larger Grad's moment system—which includes the fully contracted sixth moment as a field variable along with the 26 moments and is referred to as the system of Grad's 27-moment (G27) equations here—are computed in computer algebra software MATHEMATICA[®] and presented in appendix A for hard-sphere interaction potential. The production terms for the G26 equations can readily be found from those for the G27 equations by simply discarding the terms containing the fully contracted sixth moment. Here, it is noteworthy to point out that the present work does not have any restriction on the coefficient of restitution other than being a constant and is, consequently, expected to be applicable not only for nearly elastic granular gases but also for those having large inelasticity. With the semi-linearized G26 and G27 equations, we investigate the HCS—which has also been studied a lot theoretically, numerically as well as experimentally—of a freely cooling granular gas to show that the decay of granular temperature closely follows Haff's law (Haff 1983) while the other higher-order moments relax on a faster time scale than the granular temperature. We further study the effects of nonlinear terms of scalar fourth moment and that of linear terms of scalar sixth moment on Haff's law. By performing a Chapman–Enskog-like expansion on the G26 equations, we determine the constitutive relations for the stress and heat flux for granular gases and compare them with the existing results in the literature. We further investigate the linear stability of HCS by scrutinizing the eigenmodes of longitudinal and transverse problems associated with the G26 system and other subsystems. Similar problems related to the stability of eigenmodes have been investigated earlier by Brey *et al.* (1996) for five moment theory and by Kremer & Marques Jr. (2011) for thirteen moment theory. We find that one eigenmode from each Grad's moment theory considered in this paper is unstable for inelastic gases while other are stable, and all the eigenmodes are stable for molecular gases. Moreover, the thirteen moment theory of Kremer & Marques Jr. (2011) shows that the unstable eigenmode of the longitudinal system remains unstable below a certain value of coefficient of restitution for all wavenumbers while the present work reveals that the unstable eigenmode of the longitudinal system associated with all moment theories expect for the G13 theory becomes stable above a critical wavenumber for all values of coefficient of restitution. The present paper develops in the same spirit as that of Kremer & Marques Jr. (2011) and may be considered as an extension of Kremer & Marques Jr. (2011). The findings of the paper will be useful in better understanding of granular gases, in developing new mathematical models—such as regularized moment equations—and boundary conditions, and in capturing some intriguing features of granular gases theoretically.

The rest of the paper is structured as follows. Kinetic theory for granular gases is briefly reviewed in § 2. Grad's method of moments is outlined and applied to derive the Grad's moment systems of various orders—in particular, the system of G26 equations—for granular gases in § 3. The HCS of a freely cooling granular gas is investigated through the G26 and G27 equations in § 4 in order to discern the effects of nonlinear terms of scalar fourth moment and of linear terms of scalar sixth moment on HCS. The constitutive relations for Navier–Stokes and Fourier equations are computed through the G26 equations in § 5. The linear stability of HCS is analyzed in § 6 through the

G26 equations by decomposing them into longitudinal and transverse systems. The conclusions of the paper are given in § 7.

2. Short review of kinetic theory

We consider a dilute granular gas composed of smooth-inelastic-identical hard-spheres of mass m and diameter d . The binary collision between two such spheres having pre-collisional velocities \mathbf{c} and \mathbf{c}_1 leads to the following velocity transformation after the collision (see e.g., Brilliantov & Pöschel 2004; Rao & Nott 2008):

$$\left. \begin{aligned} \mathbf{c}' &= \mathbf{c} - \frac{1+e}{2}(\hat{\mathbf{k}} \cdot \mathbf{g})\hat{\mathbf{k}}, \\ \mathbf{c}'_1 &= \mathbf{c}_1 + \frac{1+e}{2}(\hat{\mathbf{k}} \cdot \mathbf{g})\hat{\mathbf{k}}, \end{aligned} \right\} \quad (2.1)$$

where \mathbf{c}' and \mathbf{c}'_1 are the post-collisional velocities of the respective spheres, $\mathbf{g} = \mathbf{c} - \mathbf{c}_1$ is the relative velocity, $\hat{\mathbf{k}}$ is the unit vector directed from the center of one sphere to that of other at the time of collision, and e is the coefficient of normal restitution (also, referred to as the coefficient of restitution). The coefficient of restitution e , in principal, is not a constant and usually depends on impact velocity (Bizon *et al.* 1999; Brilliantov & Pöschel 2004). Nevertheless, for simplicity, we assume that e is constant with $0 \leq e \leq 1$ in this work. The two limiting cases of $e = 0$ and $e = 1$ correspond to *sticky* and *perfectly elastic* collisions, respectively.

In kinetic theory, the state of a dilute granular gas can be described with single-particle velocity distribution function $f \equiv f(t, \mathbf{x}, \mathbf{c})$ which obeys the (inelastic) Boltzmann equation (Goldshtein & Shapiro 1995; Sela & Goldhirsch 1998; Brilliantov & Pöschel 2004)

$$\frac{\partial f}{\partial t} + c_i \frac{\partial f}{\partial x_i} + F_i \frac{\partial f}{\partial c_i} = d^2 \int_{\mathbb{R}^3} \int_{S^2} \left(\frac{1}{e^2} f'' f''_1 - f f_1 \right) (\hat{\mathbf{k}} \cdot \mathbf{g}) \Theta(\hat{\mathbf{k}} \cdot \mathbf{g}) d\hat{\mathbf{k}} d\mathbf{c}_1, \quad (2.2)$$

where Θ is the Heaviside step function, \mathbf{F} is the external force per unit mass and usually do not depend on \mathbf{c} , $f_1 \equiv f(t, \mathbf{x}, \mathbf{c}_1)$, $f'' \equiv f(t, \mathbf{x}, \mathbf{c}'')$, $f''_1 \equiv f(t, \mathbf{x}, \mathbf{c}'_1)$, the integration limits of $\hat{\mathbf{k}}$ extend over the unit sphere S^2 and Einstein summation convention is assumed over repeated indices. The velocities \mathbf{c}'' and \mathbf{c}''_1 are the pre-collisional velocities in an inverse collision and are related to the \mathbf{c} and \mathbf{c}_1 as follows (see e.g., Brilliantov & Pöschel 2004; Rao & Nott 2008).

$$\left. \begin{aligned} \mathbf{c}'' &= \mathbf{c} - \frac{1+e}{2e}(\hat{\mathbf{k}} \cdot \mathbf{g})\hat{\mathbf{k}}, \\ \mathbf{c}''_1 &= \mathbf{c}_1 + \frac{1+e}{2e}(\hat{\mathbf{k}} \cdot \mathbf{g})\hat{\mathbf{k}}, \end{aligned} \right\} \quad (2.3)$$

Owing to brevity, hereafter, we shall omit the limits of integrations. Nevertheless, the integration over any velocity space will stand for the volume integral over \mathbb{R}^3 and that over $\hat{\mathbf{k}}$ will stand for the volume integral over the unit sphere S^2 . The right-hand side (RHS) of (2.2) is referred to as the (inelastic) Boltzmann collision operator.

The hydrodynamic variables—number density $n \equiv n(t, \mathbf{x})$, macroscopic velocity $\mathbf{v} \equiv \mathbf{v}(t, \mathbf{x})$, granular temperature $T \equiv T(t, \mathbf{x})$ —are directly related to the velocity distribution function as follows.

$$n(t, \mathbf{x}) = \int f(t, \mathbf{x}, \mathbf{c}) d\mathbf{c}, \quad (2.4)$$

$$n(t, \mathbf{x}) \mathbf{v}(t, \mathbf{x}) = \int \mathbf{c} f(t, \mathbf{x}, \mathbf{c}) d\mathbf{c}, \quad (2.5)$$

$$\frac{3}{2}n(t, \mathbf{x})T(t, \mathbf{x}) = \frac{1}{2}m \int C^2 f(t, \mathbf{x}, \mathbf{c}) d\mathbf{c}, \quad (2.6)$$

where $\mathbf{C} = \mathbf{c} - \mathbf{v}(t, \mathbf{x})$ is the peculiar velocity. Here, the definition of the granular temperature—which is a measure of fluctuating kinetic energy—is adopted following the references Brilliantov & Pöschel (2004); Garzó (2013), although some authors also refer $\theta = T/m$ as granular temperature (defined as fluctuating kinetic energy per unit mass), see e.g., Lun et al. (1984); Campbell (1990); Saha & Alam (2014). It should be noted that in case of molecular gases, T in (2.6) is replaced with $k_B T_{\text{th}}$, where k_B denotes the Boltzmann constant and T_{th} is the thermodynamic temperature.

The governing equations for the hydrodynamic variables can be derived from the Boltzmann equation (2.2) as follows. Let us first introduce the moments. For a particle property, $\psi \equiv \psi(t, \mathbf{x}, \mathbf{c})$, its average value $\langle \psi \rangle \equiv \langle \psi \rangle(t, \mathbf{x})$ is defined in terms of the distribution function f as

$$\langle \psi \rangle(t, \mathbf{x}) = \frac{1}{n(t, \mathbf{x})} \int \psi(t, \mathbf{x}, \mathbf{c}) f(t, \mathbf{x}, \mathbf{c}) d\mathbf{c}. \quad (2.7)$$

The quantity on the RHS of (2.7) is referred to as the *moment* of the velocity distribution function with respect to ψ . Clearly,

$$1 = \langle 1 \rangle, \quad \mathbf{v} = \langle \mathbf{c} \rangle \quad \text{and} \quad \mathbf{T} = \left\langle \frac{1}{3} m C^2 \right\rangle. \quad (2.8)$$

The governing equation for the moment given by RHS of (2.7)—often, referred to as the moment equation for $n\langle \psi \rangle$ or the transfer equation for property ψ —is obtained by multiplying the Boltzmann equation (2.2) with ψ and integrating over the velocity space \mathbf{c} . The transfer equation for the quantity ψ reads

$$\frac{D}{Dt} \int \psi f d\mathbf{c} + \underline{\frac{\partial}{\partial x_i} \int \psi C_i f d\mathbf{c}} + \frac{\partial v_i}{\partial x_i} \int \psi f d\mathbf{c} - \int \left(\frac{D\psi}{Dt} + C_i \frac{\partial \psi}{\partial x_i} + F_i \frac{\partial \psi}{\partial c_i} \right) f d\mathbf{c} = \mathcal{P}(\psi), \quad (2.9)$$

where $\frac{D}{Dt} \equiv \frac{\partial}{\partial t} + \mathbf{v} \cdot \nabla$ is the material derivative, the underline denotes the flux term, and

$$\begin{aligned} \mathcal{P}(\psi) &= \frac{d^2}{2} \iiint (\psi' + \psi'_1 - \psi - \psi_1) f f_1 (\hat{\mathbf{k}} \cdot \mathbf{g}) \Theta(\hat{\mathbf{k}} \cdot \mathbf{g}) d\hat{\mathbf{k}} d\mathbf{c} d\mathbf{c}_1 \\ &= d^2 \iiint (\psi' - \psi) f f_1 (\hat{\mathbf{k}} \cdot \mathbf{g}) \Theta(\hat{\mathbf{k}} \cdot \mathbf{g}) d\hat{\mathbf{k}} d\mathbf{c} d\mathbf{c}_1, \end{aligned} \quad (2.10)$$

with $\psi' \equiv \psi(t, \mathbf{x}, \mathbf{c}')$ etc., is the rate of change of $\langle \psi \rangle$ per unit volume due to collisions and referred to as the *production term* or the (inelastic) *Boltzmann collision integral* corresponding to moment $\int \psi f d\mathbf{c}$. While writing (2.10), the symmetry properties of the Boltzmann collision operator (Brilliantov & Pöschel 2004; Rao & Nott 2008) have been employed. It should be noted from the transfer equation (2.9) that irrespective of the value of ψ chosen for defining a moment by (2.7), the transfer equation (2.9) will always contain an additional moment of one more order in the flux term. On substituting ψ in (2.9) with 1, c_i and $\frac{1}{3}mC^2$ successively, we get the mass, momentum and energy balance equations, respectively, which read

$$\frac{Dn}{Dt} + n \frac{\partial v_i}{\partial x_i} = 0, \quad (2.11)$$

$$n \frac{Dv_i}{Dt} + \frac{1}{m} \frac{\partial \sigma_{ij}}{\partial x_j} + \frac{1}{m} \frac{\partial(nT)}{\partial x_i} - n F_i = 0, \quad (2.12)$$

$$\frac{3}{2} n \frac{DT}{Dt} + \frac{\partial q_i}{\partial x_i} + \sigma_{ij} \frac{\partial v_i}{\partial x_j} + n T \frac{\partial v_i}{\partial x_i} = -\mathcal{D}. \quad (2.13)$$

In (2.12) and (2.13), $\sigma_{ij} \equiv \sigma_{ij}(t, \mathbf{x})$ and $q_i \equiv q_i(t, \mathbf{x})$ are the component of stress tensor and heat flux, respectively, and—following the notations of [Struchtrup \(2005\)](#)—these are given by

$$\sigma_{ij} = m \int C_{\langle i} C_{j \rangle} f \, d\mathbf{c} \quad \text{and} \quad q_i = \frac{1}{2} m \int C^2 C_i f \, d\mathbf{c}, \quad (2.14)$$

where the angle brackets around the indices denote the symmetric and traceless part of the tensor ([Struchtrup 2005](#)), and \mathcal{D} in (2.13) is the dissipation due to inelastic collisions:

$$\mathcal{D} = -\frac{m d^2}{4} \iiint \left((C')^2 + (C'_1)^2 - C^2 - C_1^2 \right) f f_1 (\hat{\mathbf{k}} \cdot \mathbf{g}) \Theta(\hat{\mathbf{k}} \cdot \mathbf{g}) \, d\hat{\mathbf{k}} \, d\mathbf{c} \, d\mathbf{c}_1. \quad (2.15)$$

Note that the RHSs of (2.11) and (2.12) vanish due to conservation of mass and momentum; however, the energy is not conserved due to dissipative collisions resulting into non vanishing RHS in (2.13). It is worth pointing out that the stress and heat flux appearing in (2.12) and (2.13)—in general—have non-vanishing collisional contributions in addition to the usual kinetic contribution given by (2.14) ([Brey *et al.* 1997](#); [Garzó & Dufty 1999](#); [Rao & Nott 2008](#); [Garzó 2013](#)). However, for dilute granular gases, the kinetic contributions to the stress and heat flux dominate over their respective collisional transfer contributions, and therefore the collisional transfer contributions to the stress and heat flux can be neglected for dilute granular gases ([Brilliantov & Pöschel 2004](#)). In any case, since (2.12) and (2.13) are obtained here by taking the velocity moments of the distribution function—which is essentially the idea of Grad’s moment method too, only kinetic contributions to the stress and heat flux will emerge in the equations. The collisional contributions to stress and heat flux, if required, must be computed separately ([Garzó 2013](#)).

Obviously, the system of equations (2.11)–(2.13) in hydrodynamic variable n , v_i and T is not closed, since it contains the unknowns σ_{ij} , q_i and \mathcal{D} , and in order to deal with this system further one must close it. Here, we employ Grad’s method of moments ([Grad 1949b](#)) in order to obtain a closed system of equations.

3. Grad’s method of moments

The function ψ in (2.7) can be chosen in infinitely many ways. Therefore, the transfer equation (2.9) leads to infinite hierarchy of moment equations. However, in practice, only a finite number of moment equations obtained by truncating the infinite hierarchy of moment equations at a certain level are used. Nonetheless, this truncated system of equation is not closed due to the (underlined) flux term in (2.9). In order to obtain a closed (finite) system of moment equations, [Grad \(1949b\)](#) expanded the velocity distribution function f in a finite linear combination of the N -dimensional Hermite polynomials ([Grad 1949a](#)) in peculiar velocity and he computed the unknown coefficients in the expansion in terms of the considered moments by satisfying their definitions with the approximated distribution function. This method of obtaining a closed set of moment equations is referred to as *Grad’s method of moments* and its details can be found in [Grad \(1949b\)](#) and in many standard textbooks, see e.g., [Chapman & Cowling \(1970\)](#); [Struchtrup \(2005\)](#).

On including the governing equations for stress (σ_{ij}) and heat flux (q_i) into the system of mass, momentum and energy balance equations (2.11)–(2.13), one obtains the well-known 13-moment equations (in three dimension). Here, we want to derive and explore the G26 equations for dilute granular flows. To this end, let us first introduce the general form of a moment. The typical form of ψ is $m C^{2a} C_{\langle i_1} C_{i_2} \dots C_{i_n \rangle}$, where $a, n \in \mathbb{N}_0$ and the angle brackets around the indices again denote the symmetric and traceless part of the corresponding quantity (Struchtrup 2005). Thus, a general moment is given by

$$u_{i_1 i_2 \dots i_n}^a = m \int C^{2a} C_{\langle i_1} C_{i_2} \dots C_{i_n \rangle} f \, d\mathbf{c}, \quad a, n \in \mathbb{N}_0. \quad (3.1)$$

Clearly,

$$u^0 = m n = \rho, \quad u_i^0 = 0, \quad u^1 = 3 n T = 3 \rho \theta, \quad u_{ij}^0 = \sigma_{ij}, \quad u_i^1 = 2 q_i, \quad (3.2)$$

where $\rho = m n$ is the mass density and $\theta = T/m$.

3.1. 26-moment equations

In addition to the well-known 13 moments, the system of 26-moment equations include full third rank tensor and one- and full-traces of the fourth moment (i.e., the 26-moment equations include the moments $n, v_i, T, \sigma_{ij}, q_i, u_{ijk}^0, u_{ij}^1, u^2$). The system of G26 equations is obtained by substituting ψ in (2.9) with $1, c_i, \frac{1}{2} m C^2, m C_{\langle i} C_{j \rangle}, \frac{1}{2} m C^2 C_i, m C_{\langle i} C_j C_{k \rangle}, m C^2 C_{\langle i} C_{j \rangle}$ and $m C^4$ successively. The system of 26-moment equations consists of the mass, momentum and energy balance equations (2.11)–(2.13) and other higher-order moment equations, which on using the abbreviations

$$m_{ijk} = u_{ijk}^0, \quad R_{ij} = u_{ij}^1 - 7\theta\sigma_{ij}, \quad \Delta = u^2 - 15\rho\theta^2, \quad (3.3)$$

read

$$\frac{D\sigma_{ij}}{Dt} + \frac{\partial m_{ijk}}{\partial x_k} + \frac{4}{5} \frac{\partial q_{\langle i}}{\partial x_{j \rangle}} + \sigma_{ij} \frac{\partial v_k}{\partial x_k} + 2\sigma_{k\langle i} \frac{\partial v_{j \rangle}}{\partial x_k} + 2\rho\theta \frac{\partial v_{\langle i}}{\partial x_{j \rangle}} = \mathcal{P}_{ij}^0, \quad (3.4)$$

$$\begin{aligned} \frac{Dq_i}{Dt} + \frac{1}{2} \frac{\partial R_{ij}}{\partial x_j} + \frac{1}{6} \frac{\partial \Delta}{\partial x_i} + \theta \frac{\partial \sigma_{ij}}{\partial x_j} + \frac{5}{2} \sigma_{ij} \frac{\partial \theta}{\partial x_j} + \frac{5}{2} \rho\theta \frac{\partial \theta}{\partial x_i} + m_{ijk} \frac{\partial v_j}{\partial x_k} \\ - \sigma_{ij} \frac{1}{\rho} \left(\frac{\partial \sigma_{jk}}{\partial x_k} + \theta \frac{\partial \rho}{\partial x_j} \right) + \frac{7}{5} q_i \frac{\partial v_j}{\partial x_j} + \frac{7}{5} q_j \frac{\partial v_i}{\partial x_j} + \frac{2}{5} q_j \frac{\partial v_j}{\partial x_i} = \frac{1}{2} \mathcal{P}_i^1, \end{aligned} \quad (3.5)$$

$$\begin{aligned} \frac{Dm_{ijk}}{Dt} + \frac{\partial u_{ijkl}^0}{\partial x_l} + \frac{3}{7} \frac{\partial R_{\langle ij}}{\partial x_{k \rangle}} + 3\theta \frac{\partial \sigma_{\langle ij}}{\partial x_{k \rangle}} - 3 \frac{1}{\rho} \sigma_{\langle ij} \left(\frac{\partial \sigma_{k \rangle l}}{\partial x_l} + \theta \frac{\partial \rho}{\partial x_{k \rangle}} \right) \\ + m_{ijk} \frac{\partial v_l}{\partial x_l} + 3m_{l\langle ij} \frac{\partial v_{k \rangle}}{\partial x_l} + \frac{12}{5} q_{\langle i} \frac{\partial v_{j \rangle}}{\partial x_k} = \mathcal{P}_{ijk}^0, \end{aligned} \quad (3.6)$$

$$\begin{aligned}
& \frac{DR_{ij}}{Dt} + 2u_{ijkl}^0 \frac{\partial v_k}{\partial x_l} + \frac{\partial u_{ijk}^1}{\partial x_k} + \frac{2}{5} \frac{\partial u_{\langle i}^2}{\partial x_{j\rangle}} + R_{ij} \frac{\partial v_k}{\partial x_k} - \frac{28}{5} \theta \frac{\partial q_{\langle i}}{\partial x_{j\rangle}} - \frac{28}{5} q_{\langle i} \frac{\partial \theta}{\partial x_{j\rangle}} \\
& + 4\theta \sigma_{k\langle i} \frac{\partial v_k}{\partial x_{j\rangle}} + 4\theta \sigma_{k\langle i} \frac{\partial v_{j\rangle}}{\partial x_k} - \frac{8}{3} \theta \sigma_{ij} \frac{\partial v_k}{\partial x_k} - \frac{14}{3} \frac{1}{\rho} \sigma_{ij} \frac{\partial q_k}{\partial x_k} - \frac{14}{3} \frac{1}{\rho} \sigma_{ij} \sigma_{kl} \frac{\partial v_k}{\partial x_l} \\
& - 7\theta \frac{\partial m_{ijk}}{\partial x_k} + \frac{6}{7} R_{\langle ij} \frac{\partial v_{k\rangle}}{\partial x_k} + \frac{4}{5} R_{k\langle i} \frac{\partial v_k}{\partial x_{j\rangle}} + 2R_{k\langle i} \frac{\partial v_{j\rangle}}{\partial x_k} + \frac{14}{15} \Delta \frac{\partial v_{\langle i}}{\partial x_{j\rangle}} \\
& - 2m_{ijk} \frac{\partial \theta}{\partial x_k} - 2 \frac{1}{\rho} m_{ijk} \left(\frac{\partial \sigma_{kl}}{\partial x_l} + \theta \frac{\partial \rho}{\partial x_k} \right) - \frac{28}{5} \frac{1}{\rho} q_{\langle i} \left(\frac{\partial \sigma_{j\rangle k}}{\partial x_k} + \theta \frac{\partial \rho}{\partial x_{j\rangle}} \right) \\
& = \mathcal{P}_{ij}^1 - 7\theta \mathcal{P}_{ij}^0 - \frac{14}{3} \frac{1}{\rho} \sigma_{ij} \left(\frac{1}{2} \mathcal{P}^1 \right), \tag{3.7}
\end{aligned}$$

$$\begin{aligned}
& \frac{D\Delta}{Dt} + \frac{\partial u_i^2}{\partial x_i} - 20\theta \frac{\partial q_i}{\partial x_i} - 8q_i \frac{\partial \theta}{\partial x_i} + \frac{7}{3} \Delta \frac{\partial v_i}{\partial x_i} + 4R_{ij} \frac{\partial v_i}{\partial x_j} \\
& + 8\theta \sigma_{ij} \frac{\partial v_i}{\partial x_j} - 8 \frac{1}{\rho} q_i \left(\frac{\partial \sigma_{ij}}{\partial x_j} + \theta \frac{\partial \rho}{\partial x_i} \right) = \mathcal{P}^2 - 20\theta \left(\frac{1}{2} \mathcal{P}^1 \right), \tag{3.8}
\end{aligned}$$

where

$$\begin{aligned}
\mathcal{P}_{i_1 i_2 \dots i_n}^a &= m d^2 \iint \left((C')^{2a} C'_{\langle i_1} C'_{i_2} \dots C'_{i_n \rangle} - C^{2a} C_{\langle i_1} C_{i_2} \dots C_{i_n \rangle} \right) \\
&\quad \times f f_1(\hat{\mathbf{k}} \cdot \mathbf{g}) \Theta(\hat{\mathbf{k}} \cdot \mathbf{g}) d\hat{\mathbf{k}} d\mathbf{c} d\mathbf{c}_1 \tag{3.9}
\end{aligned}$$

are the production terms. Notice that $\mathcal{P}^0 = \mathcal{P}_i^0 = 0$ due to mass and momentum conservation, and $\frac{1}{2} \mathcal{P}^1 = -\mathcal{D}$.

In (3.3), Δ has been defined as the difference of the full trace of fourth moment to its value computed with the Maxwellian distribution function

$$f_M \equiv f_M(t, \mathbf{x}, \mathbf{c}) = n \left(\frac{1}{2\pi\theta} \right)^{3/2} \exp \left(-\frac{C^2}{2\theta} \right), \tag{3.10}$$

and R_{ij} is defined as the difference of the one trace of fourth moment to its value computed with the Grad's 13-moment (G13) distribution function so that the quantities m_{ijk} , R_{ij} and Δ vanish for the G13 theory. It may be noted that the value of the full trace of fourth moment u^2 when computed either with Maxwellian distribution function or with the G13 distribution function is $15\rho\theta^2$.

3.2. Grad's 26-moment closure

Clearly, the system of 26-moment equations (eqs. (2.11)–(2.13) and (3.4)–(3.8)) is not closed, since it contains the unknown higher-order moments u_{ijkl}^0 , u_i^2 and u_{ijk}^1 , and on top of that the production terms are also not known. The system is closed with the Grad distribution function based on the 26 moments considered, which is referred to as the G26 distribution function and reads

$$\begin{aligned}
f_{|G26} &= f_M \left[1 + \frac{1}{2} \frac{\sigma_{ij}}{\rho\theta^2} C_i C_j + \frac{1}{5} \frac{q_i}{\rho\theta^2} C_i \left(\frac{C^2}{\theta} - 5 \right) + \frac{1}{6} \frac{m_{ijk}}{\rho\theta^3} C_i C_j C_k \right. \\
&\quad \left. + \frac{1}{28} \frac{R_{ij}}{\rho\theta^3} C_i C_j \left(\frac{C^2}{\theta} - 7 \right) + \frac{1}{8} \frac{\Delta}{\rho\theta^2} \left(1 - \frac{2}{3} \frac{C^2}{\theta} + \frac{1}{15} \frac{C^4}{\theta^2} \right) \right]. \tag{3.11}
\end{aligned}$$

Insertion of the G26 distribution function (3.11) into the definitions of higher-order moments u_{ijkl}^0 , u_i^2 and u_{ijk}^1 , and into the production terms (3.9) expresses them in terms

of the considered 26 moments. The unknown higher-order moments u_{ijkl}^0 , u_i^2 and u_{ijk}^1 turn into

$$u_{ijkl|G26}^0 = 0, \quad u_{i|G26}^2 = 28\theta q_i, \quad \text{and} \quad u_{ijk|G26}^1 = 9\theta m_{ijk}, \quad (3.12)$$

where the subscript “|G26” just denotes that these moments are evaluated with the G26 distribution function (3.11). Unfortunately, the production terms (3.9) are still not easy to evaluate by hand. The two authors of the present paper implemented the strategy for computing the production terms into computer algebra software MATHEMATICA[®] and obtained the fully nonlinear production terms associated with the G26 equations for dilute granular gases of smooth hard-spheres. The details of the computation can be found in Gupta & Torrilhon (2012) and the source code for the computation is provided as supplementary material with the present paper. Interested readers are also referred to Gupta & Torrilhon (2015a,b); Gupta (2015) for deriving the higher-order moment equations and for learning the computation of production terms in case of molecular gaseous mixtures, which might be useful in developing higher-order moment theories for mixtures of granular materials. For the sake of completeness, we provide the production terms associated with the G26 equations (eqs. (2.11)–(2.13) and (3.4)–(3.8)) in appendix A; the production terms associated with the G26 equations are (A1)–(A6) on taking $\Xi = 0$ and ignoring (A7). Notice from (A1) that the cooling rate computed via the G26 equations is given by

$$\begin{aligned} \mathcal{D} = & \frac{5}{8}(1 - e^2) \nu n T \left(1 + \frac{1}{80} \frac{\Delta}{\rho \theta^2} + \frac{1}{25600} \frac{\Delta^2}{\rho^2 \theta^4} + \frac{1}{40} \frac{\sigma_{ij} \sigma_{ij}}{\rho^2 \theta^2} \right. \\ & \left. + \frac{1}{200} \frac{q_i q_i}{\rho^2 \theta^3} + \frac{1}{1680} \frac{m_{ijk} m_{ijk}}{\rho^2 \theta^3} + \frac{3}{31360} \frac{R_{ij} R_{ij}}{\rho^2 \theta^4} - \frac{1}{560} \frac{\sigma_{ij} R_{ij}}{\rho^2 \theta^3} \right), \end{aligned} \quad (3.13)$$

where

$$\nu = \frac{16}{5} \sqrt{\pi} n d^2 \sqrt{\theta} \quad (3.14)$$

is the collision frequency. From (3.13), one can see that the dissipation computed via the G26 equations is also proportional to $(1 - e^2)$ as obtained in previous studies, see e.g., Sela & Goldhirsch (1998); van Noije & Ernst (1998); Brilliantov & Pöschel (2004); Kremer & Marques Jr. (2011), and it vanishes for molecular gases ($e = 1$) resulting into conservation of energy. Furthermore, on dropping the underlined nonlinear terms in (2.15), the expression for the dissipation matches with that in Kremer & Marques Jr. (2011). Notice that Δ used in the present work relates to Δ of Kremer & Marques Jr. (2011)—which is denoted with Δ_{KM} here—by $\Delta_{KM} = \Delta/(15\rho\theta^2)$.

3.3. Various Grad’s moment systems

Equations (2.11)–(2.13) and (3.4)–(3.8) along with (A1)–(A6) form the system of G26 equations. Various Grad’s moment systems may be obtained from the system of G26 equations.

(i) The system of well-known G13 equations contains the balance equations for variables $n, v_i, T, \sigma_{ij}, q_i$, i.e., the system of G13 equations consists of equations (2.11)–(2.13), (3.4) and (3.5) along with (A1)–(A3) and $m_{ijk} = R_{ij} = \Delta = 0$.

(ii) The system of G14 equations contains the balance equations for variables $n, v_i, T, \sigma_{ij}, q_i, \Delta$, i.e., the system of G14 equations includes equations (2.11)–(2.13), (3.4), (3.5) and (3.8) along with (A1)–(A3), (A6) and $m_{ijk} = R_{ij} = 0$.

(iii) The system of G20 equations contains the balance equations for variables

$n, v_i, T, \sigma_{ij}, q_i, m_{ijk}$, i.e., the system of G20 equations includes equations (2.11)–(2.13) and (3.4), (3.5), (3.6) along with (A 1)–(A 4) and $R_{ij} = \Delta = 0$.

(iv) The system of G21 equations contains the balance equations for variables $n, v_i, T, \sigma_{ij}, q_i, m_{ijk}, \Delta$, i.e., the system of G21 equations includes equations (2.11)–(2.13), (3.4)–(3.6) and (3.8) along with (A 1)–(A 4), (A 6) and $R_{ij} = 0$.

It is commonly accepted that the dependence of heat flux on the density gradient in addition to the temperature gradient is akin to inclusion of the full trace of the fourth moment into the moment system (Kremer & Marques Jr. 2011; Garzó 2013). In that sense, the G13 and G20 theories for granular flows may not lead to meaningful results. Nevertheless, we shall also include them in this study for comparison purposes.

4. Homogeneous cooling state

The state of a granular gas when in the absence of any external forces its (granular) temperature decays continuously but its spatial homogeneity is maintained is termed as *homogeneous cooling state* (Brilliantov & Pöschel 2004). In this section, we study the homogeneous cooling state of a granular gas with Grad's moment equations. We assume a spatially homogeneous state (i.e., $\frac{\partial(\cdot)}{\partial x_i} = 0$) without any external force acting on the particles of the granular gas (i.e., $\mathbf{F} = \mathbf{0}$). Furthermore, following Kremer & Marques Jr. (2011), in the production terms (eqs. (A 1)–(A 6)), we shall retain only those nonlinear terms which are the product of Δ and a vector or a tensor, and all other nonlinear terms are simply ignored. This means that we are focusing our attention on the early evolution stage of homogeneously cooling granular gas. The G26 equations in the zero external force case and with aforementioned simplification of the production terms read

$$\frac{Dn}{Dt} + n \frac{\partial v_i}{\partial x_i} = 0, \quad (4.1)$$

$$n \frac{Dv_i}{Dt} + \frac{1}{m} \frac{\partial \sigma_{ij}}{\partial x_j} + \frac{1}{m} \frac{\partial(nT)}{\partial x_i} = 0, \quad (4.2)$$

$$\frac{3}{2} n \frac{DT}{Dt} + \frac{\partial q_i}{\partial x_i} + \sigma_{ij} \frac{\partial v_i}{\partial x_j} + n T \frac{\partial v_i}{\partial x_i} = -\frac{5}{8} (1 - e^2) \nu n T \left(1 + \frac{1}{80} \frac{\Delta}{\rho \theta^2} \right), \quad (4.3)$$

$$\frac{D\sigma_{ij}}{Dt} + \frac{\partial m_{ijk}}{\partial x_k} + \frac{4}{5} \frac{\partial q_{\langle i}}{\partial x_{j\rangle}} + \sigma_{ij} \frac{\partial v_k}{\partial x_k} + 2\sigma_{k\langle i} \frac{\partial v_{j\rangle}}{\partial x_k} + 2\rho\theta \frac{\partial v_{\langle i}}{\partial x_{j\rangle}} \quad (4.4)$$

$$= -\frac{(1+e)(3-e)}{4} \nu \left[\left(1 - \frac{1}{480} \frac{\Delta}{\rho \theta^2} \right) \sigma_{ij} + \frac{1}{28} \left(1 + \frac{1}{160} \frac{\Delta}{\rho \theta^2} \right) \frac{R_{ij}}{\theta} \right], \quad (4.5)$$

$$\begin{aligned} & \frac{Dq_i}{Dt} + \frac{1}{2} \frac{\partial R_{ij}}{\partial x_j} + \frac{1}{6} \frac{\partial \Delta}{\partial x_i} + \theta \frac{\partial \sigma_{ij}}{\partial x_j} + \frac{5}{2} \sigma_{ij} \frac{\partial \theta}{\partial x_j} + \frac{5}{2} \rho \theta \frac{\partial \theta}{\partial x_i} + m_{ijk} \frac{\partial v_j}{\partial x_k} \\ & - \sigma_{ij} \frac{1}{\rho} \left(\frac{\partial \sigma_{jk}}{\partial x_k} + \theta \frac{\partial \rho}{\partial x_j} \right) + \frac{7}{5} q_i \frac{\partial v_j}{\partial x_j} + \frac{7}{5} q_j \frac{\partial v_i}{\partial x_j} + \frac{2}{5} q_j \frac{\partial v_j}{\partial x_i} \\ & = -\frac{(1+e)}{48} \nu \left[(49 - 33e) + \frac{(19 - 3e)}{480} \frac{\Delta}{\rho \theta^2} \right] q_i, \end{aligned} \quad (4.6)$$

$$\begin{aligned} & \frac{Dm_{ijk}}{Dt} + \frac{3}{7} \frac{\partial R_{\langle ij}}{\partial x_k} + 3\theta \frac{\partial \sigma_{\langle ij}}{\partial x_k} - 3 \frac{1}{\rho} \sigma_{\langle ij} \left(\frac{\partial \sigma_{k\rangle l}}{\partial x_l} + \theta \frac{\partial \rho}{\partial x_k} \right) + m_{ijk} \frac{\partial v_l}{\partial x_l} \\ & + 3m_{l\langle ij} \frac{\partial v_k \rangle}{\partial x_l} + \frac{12}{5} q_{\langle i} \frac{\partial v_j}{\partial x_k} = - \frac{3(1+e)(3-e)}{8} \nu \left(1 - \frac{1}{1120} \frac{\Delta}{\rho \theta^2} \right) m_{ijk}, \end{aligned} \quad (4.7)$$

$$\begin{aligned} & \frac{DR_{ij}}{Dt} + R_{ij} \frac{\partial v_k}{\partial x_k} + \frac{28}{5} \theta \frac{\partial q_{\langle i}}{\partial x_j} + \frac{28}{5} q_{\langle i} \frac{\partial \theta}{\partial x_j} + 4\theta \sigma_{k\langle i} \frac{\partial v_k}{\partial x_j} \\ & + 4\theta \sigma_{k\langle i} \frac{\partial v_j \rangle}{\partial x_k} - \frac{8}{3} \theta \sigma_{ij} \frac{\partial v_k}{\partial x_k} - \frac{14}{3} \frac{1}{\rho} \sigma_{ij} \frac{\partial q_k}{\partial x_k} - \frac{14}{3} \frac{1}{\rho} \sigma_{ij} \sigma_{kl} \frac{\partial v_k}{\partial x_l} \\ & + 2\theta \frac{\partial m_{ijk}}{\partial x_k} + \frac{6}{7} R_{\langle ij} \frac{\partial v_k \rangle}{\partial x_k} + \frac{4}{5} R_{k\langle i} \frac{\partial v_k \rangle}{\partial x_j} + 2R_{k\langle i} \frac{\partial v_j \rangle}{\partial x_k} + \frac{14}{15} \Delta \frac{\partial v_{\langle i}}{\partial x_j} \\ & + 7m_{ijk} \frac{\partial \theta}{\partial x_k} - 2 \frac{1}{\rho} m_{ijk} \left(\frac{\partial \sigma_{kl}}{\partial x_l} + \theta \frac{\partial \rho}{\partial x_k} \right) - \frac{28}{5} \frac{1}{\rho} q_{\langle i} \left(\frac{\partial \sigma_{j\rangle k}}{\partial x_k} + \theta \frac{\partial \rho}{\partial x_j} \right) \\ & = - \frac{(1+e)}{336} \nu \left[\left\{ (436 - 267e + 66e^2 - 30e^3) - \frac{(52 - 27e + 66e^2 - 30e^3)}{480} \frac{\Delta}{\rho \theta^2} \right\} R_{ij} \right. \\ & \quad \left. - 28 \left\{ (11 - 2e - 22e^2 + 10e^3) + \frac{(202 - 207e - 66e^2 + 30e^3)}{480} \frac{\Delta}{\rho \theta^2} \right\} \theta \sigma_{ij} \right], \end{aligned} \quad (4.8)$$

$$\begin{aligned} & \frac{D\Delta}{Dt} + 8\theta \frac{\partial q_i}{\partial x_i} + 20q_i \frac{\partial \theta}{\partial x_i} + \frac{7}{3} \Delta \frac{\partial v_i}{\partial x_i} + 4R_{ij} \frac{\partial v_i}{\partial x_j} + 8\theta \sigma_{ij} \frac{\partial v_i}{\partial x_j} - 8 \frac{1}{\rho} q_i \left(\frac{\partial \sigma_{ij}}{\partial x_j} + \theta \frac{\partial \rho}{\partial x_i} \right) \\ & = \frac{5(1+e)}{4} \nu \rho \theta^2 \left[(1-e)(1-2e^2) - \frac{(241 - 177e + 30e^2 - 30e^3)}{240} \frac{\Delta}{\rho \theta^2} \right]. \end{aligned} \quad (4.9)$$

In G26 system (4.1)–(4.9), it is—often—expedient to use a dimensionless field variable $\bar{\Delta} = \frac{\Delta}{\rho \theta^2}$ instead of the field variable Δ . The governing equation for $\bar{\Delta}$, which can be obtained from (4.1), (4.3) and (4.9), reads

$$\begin{aligned} & \frac{D\bar{\Delta}}{Dt} + 8 \left(1 - \frac{1}{6} \bar{\Delta} \right) \frac{1}{\rho \theta} \left(\frac{\partial q_i}{\partial x_i} + \sigma_{ij} \frac{\partial v_i}{\partial x_j} \right) \\ & + \frac{1}{\rho \theta^2} \left[20q_i \frac{\partial \theta}{\partial x_i} + 4R_{ij} \frac{\partial v_i}{\partial x_j} - 8 \frac{1}{\rho} q_i \left(\frac{\partial \sigma_{ij}}{\partial x_j} + \theta \frac{\partial \rho}{\partial x_i} \right) \right] \\ & = \frac{5(1+e)}{4} \nu \left[(1-e)(1-2e^2) - \frac{(81 - 17e + 30e^2 - 30e^3)}{240} \bar{\Delta} + \frac{(1-e)}{120} \bar{\Delta}^2 \right]. \end{aligned} \quad (4.10)$$

The G26 system in terms of $\bar{\Delta}$ shall be used while analyzing its linear stability in §6.

On introducing the scaling

$$\left. \begin{aligned} n_* &= \frac{n}{n_0}, \quad v_i^* = \frac{v_i}{\sqrt{\theta_0}}, \quad T_* = \frac{T}{T_0}, \quad \sigma_{ij}^* = \frac{\sigma_{ij}}{n_0 T_0}, \quad q_i^* = \frac{q_i}{n_0 T_0 \sqrt{\theta_0}}, \\ m_{ijk}^* &= \frac{m_{ijk}}{n_0 T_0 \sqrt{\theta_0}}, \quad R_{ij}^* = \frac{R_{ij}}{n_0 T_0 \theta_0}, \quad \Delta_* = \frac{\Delta}{n_0 T_0 \theta_0}, \quad t_* = \nu_0 t \\ \text{with } \nu_0 &= \frac{16}{5} \sqrt{\pi} n_0 d^2 \sqrt{\theta_0}, \quad \theta_0 = \frac{T_0}{m}, \quad n(0) = n_0 \quad \text{and} \quad T(0) = T_0, \end{aligned} \right\} \quad (4.11)$$

the G26 equations in the HCS (i.e., $\frac{\partial(\cdot)}{\partial x_i} = 0$) reduce to

$$\frac{dn_*}{dt_*} = 0, \quad (4.12)$$

$$\frac{dv_i^*}{dt_*} = 0, \quad (4.13)$$

$$\frac{dT_*}{dt_*} = -\frac{5}{12}(1-e^2)n_*T_*^{3/2}\left(1 + \frac{1}{80}\frac{\Delta_*}{n_*T_*^2}\right), \quad (4.14)$$

$$\frac{d\sigma_{ij}^*}{dt_*} = -\frac{(1+e)(3-e)}{4}n_*\sqrt{T_*}\left[\left(1 - \frac{1}{480}\frac{\Delta_*}{n_*T_*^2}\right)\sigma_{ij}^* + \frac{1}{28}\left(1 + \frac{1}{160}\frac{\Delta_*}{n_*T_*^2}\right)\frac{R_{ij}^*}{T_*}\right], \quad (4.15)$$

$$\frac{dq_i^*}{dt_*} = -\frac{(1+e)}{48}n_*\sqrt{T_*}\left[\left(49 - 33e\right) + \frac{(19-3e)}{480}\frac{\Delta_*}{n_*T_*^2}\right]q_i^*, \quad (4.16)$$

$$\frac{dm_{ijk}^*}{dt_*} = -\frac{3(1+e)(3-e)}{8}n_*\sqrt{T_*}\left(1 - \frac{1}{1120}\frac{\Delta_*}{n_*T_*^2}\right)m_{ijk}^*, \quad (4.17)$$

$$\begin{aligned} \frac{dR_{ij}^*}{dt_*} = & -\frac{(1+e)}{336}n_*\sqrt{T_*}\left[\left\{(436 - 267e + 66e^2 - 30e^3)\right.\right. \\ & \left. - \frac{(52 - 27e + 66e^2 - 30e^3)}{480}\frac{\Delta_*}{n_*T_*^2}\right\}R_{ij}^* \\ & \left. - 28\left\{(11 - 2e - 22e^2 + 10e^3) + \frac{(202 - 207e - 66e^2 + 30e^3)}{480}\frac{\Delta_*}{n_*T_*^2}\right\}T_*\sigma_{ij}^*\right], \end{aligned} \quad (4.18)$$

$$\frac{d\Delta_*}{dt_*} = \frac{5(1+e)}{4}n_*^2T_*^{5/2}\left[(1-e)(1-2e^2) - \frac{(241 - 177e + 30e^2 - 30e^3)}{240}\frac{\Delta_*}{n_*T_*^2}\right]. \quad (4.19)$$

4.1. Haff's law

By following heuristic approach, [Haff \(1983\)](#) discovered that in a cooling granular gas (with constant coefficient of normal restitution), the decay rate of granular temperature is given by

$$\frac{dT}{dt} \propto -\bar{n}d^2(1-e^2)T^{3/2}, \quad (4.20)$$

where \bar{n} is the average number density. The solution of (4.20) is given by

$$T(t) = \frac{T(0)}{(1+t/\tau_o)^2}, \quad (4.21)$$

where $\tau_o^{-1} \propto \bar{n}d^2(1-e^2)\sqrt{T_o}$ is an inverse time scale, see e.g., [Haff \(1983\)](#); [Brilliantov & Pöschel \(2004\)](#). Equation (4.21) is termed as Haff's law for evolution of the granular temperature of a freely cooling granular gas (with a constant coefficient of restitution).

On comparing (4.14) and (4.20), one readily perceives that Haff's law can be obtained from (4.14), provided $\frac{\Delta_*}{n_*T_*^2} =: \bar{\Delta}_*$ is constant or, in other words,

$$\frac{d\bar{\Delta}_*}{dt_*} = 0. \quad (4.22)$$

Note that $\bar{\Delta}_* = \bar{\Delta}$. With a constant value of $\bar{\Delta}_*$ ($= \alpha$, let us say), which is obtained

from condition (4.22), equations (4.12), (4.14) along with the initial conditions $n_*(0) = T_*(0) = 1$ yield Haff's law for evolution of the dimensionless granular temperature T_* :

$$T_*(t_*) = \frac{1}{(1 + t_*/\tau_0)^2}, \quad (4.23)$$

where

$$\tau_0^{-1} = \frac{5}{24}(1 - e^2) \left(1 + \frac{1}{80}\alpha\right) \quad (4.24)$$

is the inverse of a (dimensionless) time scale τ_0 .

It is worth pointing out that, in the light of condition (4.22), the constant α in (4.24) is an *equilibrium point* (Strogatz 1994) of a first-order ordinary differential equation

$$\frac{d\bar{\Delta}_*}{dt_*} = \frac{5(1+e)}{4} n_* \sqrt{T_*} \left[(1-e)(1-2e^2) - \frac{(81-17e+30e^2-30e^3)}{240} \bar{\Delta}_* + \frac{(1-e)}{120} \bar{\Delta}_*^2 \right], \quad (4.25)$$

which is obtained by exploiting (4.12), (4.14) and (4.19). Here, we shall discard the nonlinear term proportional to $\bar{\Delta}_*^2$ term in (4.25), although we shall analyze the effect of this term in § 4.3. On discarding $\bar{\Delta}_*^2$ term in (4.25), one readily obtains the equilibrium point—which is the constant α in (4.24)—as

$$\alpha = 15 a_2, \quad \text{where} \quad a_2 := \frac{16(1-e)(1-2e^2)}{81-17e+30e^2-30e^3} \quad (4.26)$$

is same as the coefficient of second Sonine polynomial $S_2(v^2)$ while performing Chapman–Enskog expansion, see e.g., van Noije & Ernst (1998); Brilliantov & Pöschel (2004).

4.2. Relaxation of moments in the homogeneous cooling state

It is clear from (4.12) and (4.13) that the number density n_* remains constant while the macroscopic velocity v_i^* remains zero (since there is no macroscopic velocity in the initial state) during the homogeneous cooling. Furthermore, equations (4.15)–(4.19) are coupled and, therefore need to be solved numerically for further analysis. It may also be noticed from the structure of (4.16) and (4.17) that vanishing initial conditions on q_i^* and m_{ijk}^* will result into vanishing solution for these quantities. Similarly, vanishing initial conditions on both σ_{ij}^* and R_{ij}^* will also result into zero solution for them; however, owing to the coupling on the RHSs of (4.15) and (4.18), a non-vanishing initial condition on one of them will trigger the non-vanishing solution for both of them. On the contrary, vanishing initial condition on Δ_* results into non-vanishing solution for it for all values of the coefficient of restitution except for $e = 1$ and $e = 1/\sqrt{2}$. Therefore, in the following analysis, we take the initial conditions as $n_*(0) = T_*(0) = \sigma_{ij}^*(0) = m_{ijk}^*(0) = \Delta_*(0) = 1$ and $v_i^*(0) = R_{ij}^*(0) = 0$.

Figure 1 illustrates the numerical solution for the (dimensionless) granular temperature and other higher-order moments obtained by solving the system (4.12)–(4.19) along with the aforementioned initial conditions. The solution for number density and velocity are not shown since they are just constants. Figure 1(a) exhibits the granular temperature for two values of the coefficient of restitution $e = 0.75$ (in blue color) and $e = 0.95$ (in red color). The solid lines depict the numerical solution obtained by solving the system (4.12)–(4.19) along with the aforementioned initial conditions while the symbols denote the corresponding granular temperature computed via Haff's law (4.23). Clearly, the numerical results (denoted by solid lines) are in very good agreement with those obtained via Haff's law (denoted by symbols). Moreover, it is also clear that the granular

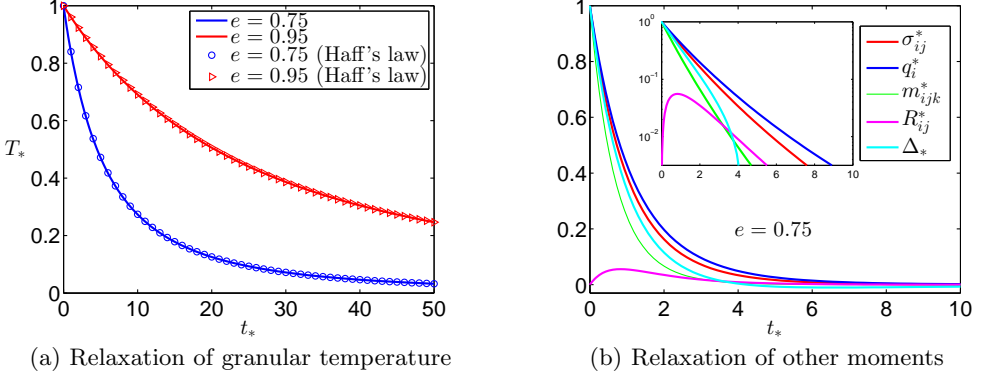


FIGURE 1. Relaxation of various moments in the homogeneous cooling state: (a) relaxation of granular temperature T_* ; lines depict solutions obtained by solving the system (4.12)–(4.19) for two values while symbols delineate Haff’s law (eq. (4.23)); the blue and red colors correspond to coefficient of restitution $e = 0.75$ and $e = 0.95$, respectively, and (b) relaxation of other moments— σ_{ij}^* , q_i^* , m_{ijk}^* , R_{ij}^* and Δ_* —for coefficient of restitution $e = 0.75$. Initial conditions are taken as $n_*(0) = T_*(0) = \sigma_{ij}^*(0) = m_{ijk}^*(0) = \Delta_*(0) = 1$ and $v_i^*(0) = R_{ij}^*(0) = 0$.

temperature relaxes faster with decreasing coefficient of normal restitution. This is due to the fact that more inelastic particles dissipate more energy during the collision in comparison to the less inelastic ones and therefore, the granular temperature of the former relaxes faster than that of the latter. The relaxation of other moments— σ_{ij}^* , q_i^* , m_{ijk}^* , R_{ij}^* and Δ_* —with time t_* for $e = 0.75$ is displayed in figure 1(b). The inset of figure 1(b) portrays the same quantities on log-scale for more clarity. It turns out that σ_{ij}^* , q_i^* , m_{ijk}^* and R_{ij}^* relax to zero much faster than the granular temperature. Although, the initial condition for R_{ij}^* is zero, it manifests non-zero solution due to the coupling on the RHSs of (4.15) and (4.18). On the one hand, σ_{ij}^* , q_i^* and m_{ijk}^* decays with time t_* from their initial values to zero; on the other hand, R_{ij}^* first increases and then relaxes to zero whereas Δ_* first decays and starts becoming negative around $t_* \approx 4.25$ and then increases back to relax to zero later, yet faster than the granular temperature. It is worth pointing out that, in contrast to the quantities plotted in figure 1(b), the quantity Δ_* —not shown here—relax to a constant negative value, but not to zero for $e = 0.75$. It may be noted from figure 1(b) that stress (red curve) decays faster than the heat flux (blue curve) which is in agreement with the result of Kremer & Marques Jr. (2011). Moreover, the decay rate of both stress (red curve) and heat flux (blue curve) is slower than all other higher moments. At small times ($t_* \lesssim 3.5$), the third moment m_{ijk}^* decays faster than Δ_* ; however for $t_* \gtrsim 3.5$, the relaxation trend seems to be faster for Δ_* followed by m_{ijk}^* and R_{ij}^* (particularly, for the initial conditions used).

4.3. Effect of nonlinear terms of scalar moment (Δ_*) on Haff’s law

In § 4.1, we obtained Haff’s law by dropping all the nonlinear terms of non-equilibrium moments (σ_{ij}^* , q_i^* , m_{ijk}^* , R_{ij}^* , Δ_*) in (4.14) and (4.19). In this subsection, we shall investigate the effect of nonlinear terms of scalar moment (Δ_*) on Haff’s law in detail.

4.3.1. Case 1: Effect of $\bar{\Delta}_*^2$ term present in (4.25)

The constant α in characteristic time scale τ_0 for temperature decay via Haff’s law (4.23) was obtained by discarding $\bar{\Delta}_*^2$ term in (4.25). We now consider (4.25) without dropping any term. Equation (4.25) has two equilibrium points for $e \neq 1$. Nevertheless,

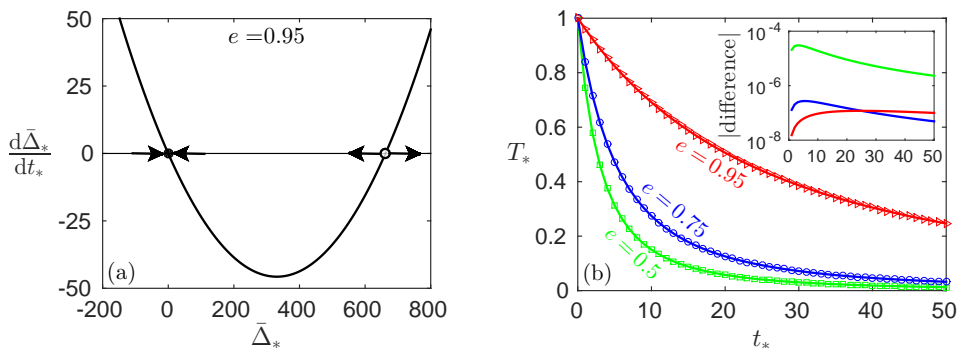


FIGURE 2. Stability of roots and Haff's law: (a) phase portrait showing stable (black filled circle) and unstable (white filled circle) equilibrium points of (4.25) and (b) temperature decay via Haff's law (4.23) with inverse time scale (4.24) for $e = 0.5, 0.75, 0.95$ shown by green, blue and red colors respectively; the continuous lines depict Haff's law corresponding to stable equilibrium point (black filled circle) while the symbols show that with constant α given in (4.26)₁ (i.e., the linear case); the inset shows the absolute difference between the temperature values in these two cases.

a simple stability analysis of these equilibrium points (see Chapter 2 of [Strogatz 1994](#)) shows that only one equilibrium point is stable whereas the other one is unstable. In the limiting case of $e \rightarrow 1$, the stable equilibrium point tends to zero while the unstable equilibrium point tends to infinity. This makes sense as (4.25) in the case of $e = 1$ has only one equilibrium point (which is zero). Furthermore, in the limiting case of $e \rightarrow 1$, the stable equilibrium point leads to infinite relaxation time τ_0 which is meaningful for molecular gases (i.e., for $e = 1$); however the unstable equilibrium point in this limit leads to a finite relaxation time which is meaningless. Owing to these reasons, we shall neglect the unstable equilibrium point.

Figure 2(a) portrays the stable equilibrium point (by black filled circle) and unstable equilibrium point (by white filled circle) for $e = 0.95$ on a phase portrait. We consider only the stable equilibrium point (marked by black filled circle) and neglect the unstable equilibrium point (marked by white filled circle). The main panel of figure 2(b) illustrates the temperature decay via Haff's law (4.23) for three values of the coefficient of restitution $e = 0.5, 0.75, 0.95$, shown by green, blue and red colors, respectively. The continuous lines depict the results obtained with the stable equilibrium point of (4.25) whereas the symbols show the corresponding results obtained with a single equilibrium point (4.26)₁ (i.e., with linear case). In the inset of figure 2(b), we also plot the corresponding absolute difference between the temperature values obtained in both the cases. It turns out that the difference is many order of magnitude smaller than the original temperature values. This difference is even smaller for more elastic particles. Thus we conclude that the $\bar{\Delta}_*^2$ term present in (4.25) do not play any significant role on Haff law.

4.3.2. Case 2: Effect of $\bar{\Delta}_*^2$ terms present in (4.14) and (4.19)

To investigate the effect of nonlinear terms of scalar moment (i.e., $\bar{\Delta}_*^2$ terms) on Haff's law one needs to include Δ^2 terms in the production terms of the energy balance equation (2.13) and Δ balance equation (3.8). On including Δ^2 terms in the production terms and introducing the scaling (4.11), the new energy and Δ_* balance equations in the

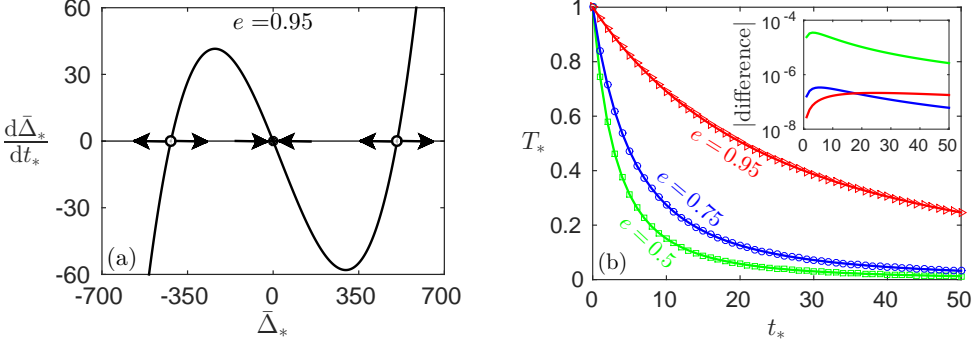


FIGURE 3. Stability of roots and Haff's law: (a) phase portrait showing stable (black filled circle) and unstable (white filled circle) equilibrium points of (4.30) and (b) temperature decay via Haff's law (4.23) with inverse time scale (4.29) for $e = 0.5, 0.75, 0.95$ shown by green, blue and red colors respectively; the continuous lines depict Haff's law corresponding to stable equilibrium point (black filled circle) while the symbols show Haff's law (4.23) with inverse time scale (4.24) and with constant α given in (4.26)₁ (i.e., the linear case); the inset shows the absolute difference between the temperature values in these two cases.

homogeneous cooling state read

$$\frac{dT_*}{dt_*} = -\frac{5}{12}(1-e^2)n_*T_*^{3/2}\left(1 + \frac{1}{80}\bar{\Delta}_* + \frac{1}{25600}\bar{\Delta}_*^2\right), \quad (4.27)$$

$$\begin{aligned} \frac{d\bar{\Delta}_*}{dt_*} = & \frac{5(1+e)}{4}n_*^2T_*^{5/2}\left[(1-e)(1-2e^2) - \frac{(241-177e+30e^2-30e^3)}{240}\bar{\Delta}_* \right. \\ & \left. - \frac{(47+81e-30e^2+30e^3)}{230400}\bar{\Delta}_*^2\right]. \end{aligned} \quad (4.28)$$

Again, for obtaining Haff's law form (4.27), $\bar{\Delta}_*$ should be a constant or, in other words, condition (4.22) must be fulfilled. With a constant value of $\bar{\Delta}_*$ ($= \beta$, let us say), eqs. (4.12) and (4.27) along with the initial conditions $n_*(0) = T_*(0) = 1$ again yield the Haff's law (4.23). However, the inverse of dimensionless characteristic time scale in this case reads

$$\tau_0^{-1} = \frac{5}{24}(1-e^2)\left(1 + \frac{1}{80}\beta + \frac{1}{25600}\beta^2\right). \quad (4.29)$$

Again, in the light of condition (4.22), the constant β in (4.29) is an equilibrium point (Strogatz 1994) of a first-order ordinary differential equation

$$\begin{aligned} \frac{d\bar{\Delta}_*}{dt_*} = & \frac{5(1+e)}{4}n_*\sqrt{T_*}\left[(1-e)(1-2e^2) - \frac{(81-17e+30e^2-30e^3)}{240}\bar{\Delta}_* \right. \\ & \left. + \frac{(1873-2001e+30e^2-30e^3)}{230400}\bar{\Delta}_*^2 + \frac{(1-e)}{38400}\bar{\Delta}_*^3\right], \end{aligned} \quad (4.30)$$

which is obtained by exploiting (4.12), (4.27) and (4.28).

Equation (4.30) has three equilibrium points for $e \neq 1$. Again, a simple stability analysis of these equilibrium points (see Chapter 2 of Strogatz 1994) shows that only one equilibrium point is stable whereas the other two are unstable. Figure 3(a) displays the stable equilibrium point (by black filled circle) and unstable equilibrium points (by white filled circles) for $e = 0.95$ on a phase portrait. In the limiting case of $e \rightarrow 1$, the stable equilibrium point tends to zero, the left unstable point tends to -480 and the right unstable equilibrium point tends to infinity. That one equilibrium point of (4.30) in the

limiting case of $e \rightarrow 1$ tends to infinity makes sense as (4.30) in the case of $e = 1$ has only two equilibrium points. Furthermore, in the limiting case of $e \rightarrow 1$, the stable equilibrium point and the left unstable equilibrium point lead to infinite relaxation time τ_0 which is meaningful for molecular gases (i.e., for $e = 1$); however the right unstable equilibrium point in this limit leads to a vanishing relaxation time which is meaningless, therefore we neglect the right unstable equilibrium point. Although, the left unstable equilibrium point lead to meaningful infinite relaxation time τ_0 in the limit $e \rightarrow 1$, its value in the limit $e \rightarrow 1$ itself is not meaningful because the equilibrium points are the steady state solutions of (4.30) and the distribution function for molecular gases (i.e., for $e = 1$) in the steady state is Maxwellian, and consequently, by definition, Δ (and hence $\bar{\Delta}_*$) must vanish in the limit $e \rightarrow 1$ and in the steady state.

Therefore, we again consider only the stable equilibrium point (marked by black filled circle) and neglect the unstable equilibrium points (marked by white filled circles). The main panel of figure 3(b) illustrates the temperature decay via Haff's law (4.23) for three values of the coefficient of restitution $e = 0.5, 0.75, 0.95$, shown by green, blue and red colors, respectively. The continuous lines depict the results obtained with the value for β in (4.29) corresponding to stable equilibrium point of (4.30) whereas the symbols show the corresponding results obtained with the value for α in (4.24) as a single equilibrium point (4.26)₁ (i.e., with linear case). In the inset of figure 3(b), we also plot the corresponding absolute difference between the temperature values obtained in both the cases. There is practically no difference in both the results as the difference is again many order of magnitude smaller than the original temperature values.

Thus, we conclude that the nonlinear terms of scalar moment (Δ) do not play any significant role on Haff law.

4.4. Effect of higher-order scalar moment on Haff's law

In this subsection, we shall analyze effect of the sixth order scalar moment u^3 , which is the full trace of the sixth order moment, on Haff's law. Nevertheless, for convenience, we introduce a new variable Ξ which is related to the sixth order scalar moment u^3 via

$$\Xi = m \int (f - f_M) (C^6 - 21 \theta C^4) d\mathbf{c} = u^3 - 105 \rho \theta^3 - 21 \theta \Delta \quad (4.31)$$

so that Ξ vanishes if it is computed with f as either Maxwellian or G13 distribution function or G26 distribution function.

We now include the governing equation for the moment Ξ to our existing 26-moment system (eqs. (2.11)–(2.13) and (3.4)–(3.8)) and close this system with the Grad distribution function (which we shall name as the G27 distribution function)

$$\begin{aligned} f_{|G27} = f_M \left[1 + \frac{1}{2} \frac{\sigma_{ij}}{\rho \theta^2} C_i C_j + \frac{1}{5} \frac{q_i}{\rho \theta^2} C_i \left(\frac{C^2}{\theta} - 5 \right) + \frac{1}{6} \frac{m_{ijk}}{\rho \theta^3} C_i C_j C_k \right. \\ \left. + \frac{1}{28} \frac{R_{ij}}{\rho \theta^3} C_i C_j \left(\frac{C^2}{\theta} - 7 \right) + \frac{1}{8} \frac{\Delta}{\rho \theta^2} \left(1 - \frac{2}{3} \frac{C^2}{\theta} + \frac{1}{15} \frac{C^4}{\theta^2} \right) \right. \\ \left. - \frac{1}{48} \frac{\Xi}{\rho \theta^3} \left(1 - \frac{C^2}{\theta} + \frac{1}{5} \frac{C^4}{\theta^2} - \frac{1}{105} \frac{C^6}{\theta^3} \right) \right]. \end{aligned} \quad (4.32)$$

We shall refer to the system of these 27-moment equations closed with the G27 distribution function as the system of G27 equations.

For our purposes, it is not necessary to derive the full G27 equations but we do need the production terms for energy balance, Δ balance and Ξ balance equations. All the production terms associated with the G27 equations are given in appendix A. In the

homogeneous cooling state, the dimensionless energy balance, Δ balance and Ξ balance equations from the system of G27 equations—on employing (4.11) and scaling $\Xi_* := \frac{\Xi}{n_0 T_0 \theta_0^2}$, and discarding all the nonlinear terms of scalar, vector or tensor moments—read

$$\frac{dT_*}{dt_*} = -\frac{5}{12}(1-e^2)n_*T_*^{3/2}\left(1 + \frac{1}{80}\bar{\Delta}_* - \frac{1}{6720}\frac{\Xi_*}{n_*T_*^3}\right), \quad (4.33)$$

$$\begin{aligned} \frac{d\bar{\Delta}_*}{dt_*} = & \frac{5(1+e)}{4}n_*^2T_*^{5/2}\left[(1-e)(1-2e^2) - \frac{(241-177e+30e^2-30e^3)}{240}\bar{\Delta}_* \right. \\ & \left. - \frac{(191-127e+10e^2-10e^3)}{6720}\frac{\Xi_*}{n_*T_*^3}\right], \end{aligned} \quad (4.34)$$

$$\begin{aligned} \frac{d\Xi_*}{dt_*} = & -\frac{15}{16}n_*^2T_*^{7/2}\left[(3-15e^2+20e^4-8e^6) \right. \\ & - \frac{(1111+384e-2739e^2-512e^3+1220e^4+280e^6)}{240}\bar{\Delta}_* \\ & \left. + \frac{(11633+2432e-4005e^2+1536e^3-3380e^4-280e^6)}{6720}\frac{\Xi_*}{n_*T_*^3}\right]. \end{aligned} \quad (4.35)$$

Again, for obtaining Haff's law form (4.33), $\bar{\Delta}_*$ and $\bar{\Xi}_* := \frac{\Xi_*}{n_*T_*^3}$ should be constants or, in other words, conditions

$$\frac{d\bar{\Delta}_*}{dt_*} = \frac{d\bar{\Xi}_*}{dt_*} = 0 \quad (4.36)$$

must be fulfilled. With constant values of $\bar{\Delta}_*$ ($= \varkappa_1$, let us say) and $\bar{\Xi}_*$ ($= \varkappa_2$, let us say), eqs. (4.12) and (4.33) along with the initial conditions $n_*(0) = T_*(0) = 1$ again yield the Haff's law (4.23). However, the inverse of dimensionless characteristic time scale now reads

$$\tau_0^{-1} = \frac{5}{24}(1-e^2)\left(1 + \frac{1}{80}\varkappa_1 - \frac{1}{6720}\varkappa_2\right). \quad (4.37)$$

In the light of condition (4.36), the constants $(\varkappa_1, \varkappa_2)$ in (4.37) are the equilibrium points $(\bar{\Delta}_*^{\text{eq}}, \bar{\Xi}_*^{\text{eq}})$ of a system of two first-order ordinary differential equations (Strogatz 1994)

$$\begin{aligned} \frac{d\bar{\Delta}_*}{dt_*} = & \frac{5(1+e)}{4}n_*\sqrt{T_*}\left[(1-e)(1-2e^2) - \frac{(81-17e+30e^2-30e^3)}{240}\bar{\Delta}_* \right. \\ & \left. - \frac{(191-127e+10e^2-10e^3)}{6720}\bar{\Xi}_* + \frac{(1-e)}{120}\bar{\Delta}_*\left(\bar{\Delta}_* - \frac{1}{84}\bar{\Xi}_*\right)\right], \end{aligned} \quad (4.38)$$

$$\begin{aligned} \frac{d\bar{\Xi}_*}{dt_*} = & -\frac{15}{16}n_*\sqrt{T_*}\left[(3-15e^2+20e^4-8e^6) \right. \\ & - \frac{(1111+384e-2739e^2-512e^3+1220e^4+280e^6)}{240}\bar{\Delta}_* \\ & + \frac{(2673+2432e+4955e^2+1536e^3-3380e^4-280e^6)}{6720}\bar{\Xi}_* \\ & \left. - \frac{(1-e^2)}{60}\bar{\Xi}_*\left(\bar{\Delta}_* - \frac{1}{84}\bar{\Xi}_*\right)\right]. \end{aligned} \quad (4.39)$$

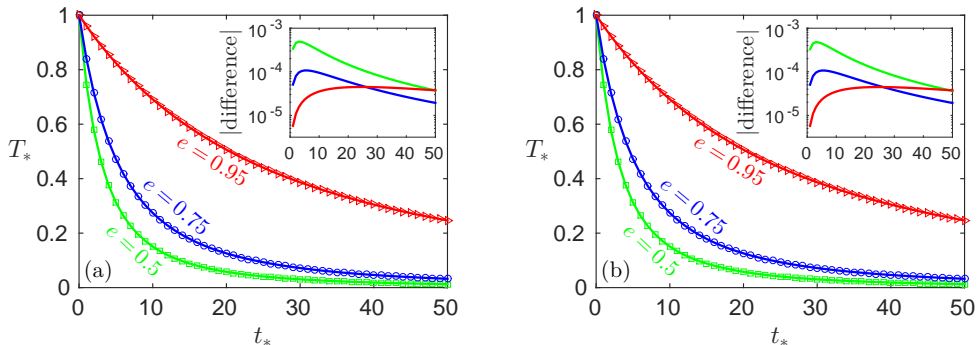


FIGURE 4. Temperature decay via Haff's law (4.23) from the linearized G27 equations (shown by the continuous lines): (a) without underbraced terms in (4.38) and (4.39), and (b) with underbraced terms in (4.38) and (4.39). The green, blue and red colors show the results for $e = 0.5, 0.75, 0.95$ respectively; the symbols show Haff's law (4.23) with inverse time scale (4.24) and with constant α given in (4.26)₁; the insets show the absolute difference between the temperature values.

The system of eqs. (4.38) and (4.39) on dropping the underbraced terms has a unique equilibrium point whereas the full system (without dropping the underbraced terms) has three equilibrium points. Nevertheless, two equilibrium points out of these three are complex for most values of e , therefore these equilibrium points are meaningless and we simply ignore them. For both the cases (without and with underbraced terms in (4.38) and (4.39)), the temperature decay via Haff's law (4.23)—with inverse time scale (4.37)—for three values of coefficient of restitution $e = 0.5, 0.75, 0.95$ is illustrated in figure 4 by green, blue and red colors, respectively. The continuous lines in figure 4(a) depict the temperature decay for the case when underbraced terms in (4.38) and (4.39) are discarded while those in figure 4(b) display the temperature decay for the case when full (4.38) and (4.39) equations are exploited. The symbols show the corresponding Haff's law (4.23) with inverse time scale (4.24) and α given in (4.26)₁. In the insets of figure 4(a) and (b), we also plot the respective absolute differences between the temperature values, and, again, there is practically no difference in the results as the differences are many order of magnitude smaller than the original temperature values.

Furthermore, in view of § 4.3, it is expected that the nonlinear terms in (4.33)–(4.35) would also have negligible effect on Haff's law. Thus, it is concluded *empirically* that the nonlinear terms of non-equilibrium moments as well as higher-order moments do not have any significant effect on Haff's law and therefore, it suffices to consider only those moment systems which consists of the fourth order scalar moment (Δ)—i.e., to consider 14- or 26-moment system—and only up to linear terms of non-equilibrium moments for analyzing Haff's law.

5. Constitutive relations for the stress and heat flux: Navier–Stokes, and Fourier laws

In this section, we shall investigate the constitutive relations for the stress and heat flux in a five moment theory associated with the first five moments: density ρ (or number density n), velocity v_i and granular temperature T . In particular, we shall compare the transport coefficients obtained with the G26 theory and those obtained with the G14 theory of Kremer & Marquies Jr. (2011).

The moment equations for the first five moments—number density n , velocity v_i

and granular temperature T —are the mass, momentum and energy balance equations, and are given by (2.11)–(2.13). The stress σ_{ij} and heat flux q_i in system (2.11)–(2.13) are not the field variables in a 5-moment theory; rather, they are the constitutive quantities which need to be computed somehow. The two widely used methods for computing the constitutive relations for the first five moment equations are the CE method (Chapman & Cowling 1970) and the Maxwellian iteration procedure (Ikenberry & Truesdell 1956). Here, we employ Chapman–Enskog-like expansion (Struchtrup 2005) on the balance equations for non-equilibrium field variables (i.e., on (4.4)–(4.9)) in the simplified system of G26 equations ((4.1)–(4.9)) to compute the constitutive relations for the stress σ_{ij} and heat flux q_i .

To this end, the RHSs of (4.4)–(4.9) are multiplied with $1/\varepsilon$, where ε is the Knudsen number, and replaced by 1 in the end of the procedure (see § 6.3 of Struchtrup 2005). The multiplication of factor $1/\varepsilon$ is equivalent of making the equations dimensionless, which introduces the factor $1/\varepsilon$ in the RHSs of these equations, and replacing ε by 1 is equivalent of writing the final results in the dimensional form. Next, all the non-equilibrium variables $\Psi \in \{\sigma_{ij}, q_i, m_{ijk}, R_{ij}, \Delta\}$ are expanded in powers of the smallness parameter, the Knudsen number ε as

$$\Psi = \Psi_{|0} + \varepsilon \Psi_{|1} + \varepsilon^2 \Psi_{|2} + \dots \quad (5.1)$$

and these expansions for the variables is substituted in (4.4)–(4.9)—after multiplying their RHSs with $1/\varepsilon$. Finally, the coefficients of each power of ε on both sides of the equations are compared. Comparing the coefficients of ε^{-1} on both sides of these equations one readily finds that $\Psi_{|0} = 0$ for $\Psi \in \{\sigma_{ij}, q_i, m_{ijk}, R_{ij}\}$ whereas

$$\Delta_{|0} = \frac{240(1-e)(1-2e^2)\rho\theta^2}{241-177e+30e^2-30e^3}. \quad (5.2)$$

Clearly, $\Delta_{|0} = 0$ in the elastic limit ($e = 0$) but nonzero for granular flows ($e \neq 0$). It may also be noted that $\Delta_{|0} \neq (15\rho\theta^2)a_2$ (cf. (4.26) and (5.2)), which was assumed the value of Δ while computing the constitutive relations via the G14 theory of Kremer & Marques Jr. (2011). This means that to zeroth order approximation, the moments σ_{ij} , q_i , m_{ijk} and R_{ij} vanish while Δ is nonzero and its value is given by the RHS of (5.2). Next, on comparing the coefficients of ε^0 on both sides of equations for stress and heat flux (eqs. (4.4) and (4.6) on multiplying the RHSs with $1/\varepsilon$ and substituting expansions (5.1); other equations are not required), one obtains the value of $\sigma_{ij|1}$ and $q_{i|1}$, which lead to the first order approximation for stress and heat flux, and on replacing ε by 1 they read

$$\sigma_{ij} = -2\mu \frac{\partial v_{\langle i}}{\partial x_{j\rangle}} \quad \text{and} \quad q_i = -\kappa \frac{\partial T}{\partial x_i} - \lambda \frac{\partial n}{\partial x_i}, \quad (5.3)$$

Equations (5.3)₁ and (5.3)₂ are the Navier–Stokes law and Fourier law, respectively. The transport coefficients: shear viscosity (μ), coefficient of thermal conductivity (κ), and coefficient λ in (5.3) are given by

$$\mu = c_\mu \frac{\sqrt{mT}}{d^2}, \quad \kappa = c_\kappa \frac{1}{d^2} \sqrt{\frac{T}{m}}, \quad \lambda = c_\lambda \frac{T}{n d^2} \sqrt{\frac{T}{m}}, \quad (5.4)$$

where

$$\left. \begin{aligned} c_\mu &= \frac{5}{16\sqrt{\pi}} \frac{a_\mu}{b_\mu}, \\ c_\kappa &= \frac{75}{\sqrt{\pi}} \frac{(273 - 209e - 34e^2 + 34e^3)}{(1+e)(23637 - 33274e + 14587e^2 - 4876e^3 + 1974e^4)}, \\ c_\lambda &= \frac{1200}{\sqrt{\pi}} \frac{(1-e)(1-2e^2)}{(1+e)(23637 - 33274e + 14587e^2 - 4876e^3 + 1974e^4)}, \end{aligned} \right\} \quad (5.5)$$

with

$$\begin{aligned} a_\mu &= 4(50145220 - 104369123e + 93420044e^2 - 62856785e^3 + 35951358e^4 \\ &\quad - 14331030e^5 + 5007864e^6 - 1466748e^7 + 234360e^8 - 55800e^9), \\ b_\mu &= (1+e)(3-e)(51863770 - 107394001e + 91917114e^2 - 56962439e^3 \\ &\quad + 31413906e^4 - 12148138e^5 + 4013504e^6 - 1186788e^7 + 180936e^8 - 43080e^9). \end{aligned}$$

In case of molecular gases ($e = 1$), the reported (exact) value of coefficient a_μ/b_μ is 1.016034 (and, hence, that of c_μ is 0.179136) (Pekeris & Alterman 1957). The G14 theory of Kremer & Marques Jr. (2011)—in this case—yields $a_\mu/b_\mu = 1$ (and $c_\mu = 5/(16\sqrt{\pi}) \approx 0.176309$) whereas the G26 theory considered in this section yields $a_\mu/b_\mu = 205/202 \approx 1.01485$ (and $c_\mu = 1025/(3232\sqrt{\pi}) \approx 0.178928$). Thus, the coefficient c_μ computed from the G14 theory differs from its realistic value 0.179136 by about 1.58% while that from the G26 theory differs only by about 0.12%, thanks to the coupling between σ_{ij} and R_{ij} in their balance equations. Furthermore, the reported value of the coefficient c_κ in Pekeris & Alterman (1957) or molecular gases ($e = 1$) is $1.025218 \times 75/(64\sqrt{\pi})$. Nevertheless, both the G14 and G26 theories in this case yield the same value $c_\kappa = 75/(64\sqrt{\pi})$ because, owing to linearization, there is no coupling of other moments in the RHS of heat flux balance equation, and consequently, the RHSs of linearized heat flux balance equations in the G14 and G26 systems are the same.

It is worth pointing out that the non-Fourier contribution (i.e., the term proportional to the number density gradient) in the Fourier law (5.3)₂ is solely due to the fact that Δ is nonzero at zeroth order of the Chapman–Enskog-like expansion, and that it depends on the density ρ and granular temperature θ . Since $\Delta|_0 = 0$ for the elastic case, this term identically vanishes in the elastic case, which can also be seen immediately from the value of c_λ in (5.5)₃. Moreover, if one considers the G13 theory, or a theory that neglects the fourth order scalar moment Δ , the density gradient term will never appear in the Fourier law. Therefore, the density gradient term in heat flux is a consequence of using higher-order scalar moments. On neglecting the nonzero value of fourth order scalar moment Δ at zeroth order, one would obtain the transport coefficients similar to those obtained by Jenkins & Richman (1985a). At this point, it is illustrative to compare the transport coefficients with those obtained by 14-moment theory of Kremer & Marques Jr. (2011). Figure 5 illustrates the variation of coefficients, c_μ , c_κ , and c_λ with coefficient of restitution e . For comparison purposes, these coefficients predicted by the G14 theory of Kremer & Marques Jr. (2011) have also been included in figure 5. From figure 5(a), it is clear that the coefficient c_μ predicted by the G14 theory of Kremer & Marques Jr. (2011) and that by the G26 theory considered in this section are qualitatively same. Nevertheless, in comparison to the G26 theory considered here, the G14 theory of Kremer & Marques Jr. (2011) underpredicts the coefficient c_μ for $0.8 \lesssim e \leq 1$ while overpredicts that for $0 \leq e \lesssim 0.8$, see figure 5(a). Figures 5(b) and (c) illustrate that the coefficients c_κ and c_λ computed with the G26 theory closely follow the

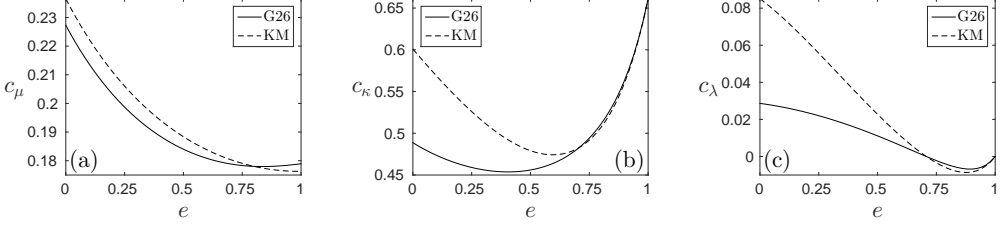


FIGURE 5. Variation of coefficients (a) c_μ , (b) c_κ and (c) c_λ with coefficient of restitution e . The solid lines depict the results obtained by Chapman–Enskog like expansion on G26 equations (performed in this paper) while the dashed lines display those obtained by Maxwellian iteration on G14 equations in Kremer & Marques Jr. (2011). The abbreviation ‘KM’ is used for the G14 theory of Kremer & Marques Jr. (2011).

respective coefficients computed with the G14 theory of Kremer & Marques Jr. (2011) for $0.7 \lesssim e \leq 1$ whereas the values of both the coefficients in case of $0 \leq e \lesssim 0.7$ are much lower with the G26 theory in comparison to those with the G14 theory of Kremer & Marques Jr. (2011). Furthermore, as pointed out before, both the G26 theory and the G14 theory of Kremer & Marques Jr. (2011) leads to the same (nonzero) value of the coefficient c_κ and to the same (zero) value of the coefficient c_λ in the elastic case ($e = 1$).

6. Linear stability analysis

In this section, we investigate the stability of the HCS due to small perturbations through various moment theories—particularly, with the G26 theory—developed in the earlier sections. We assume that the amplitudes of these perturbations are sufficiently small so that the linear analysis remains valid.

For the linear stability analysis, we decompose all the field variables into their reference values—i.e., their respective solutions in the HCS—and into perturbations from their respective solutions in the HCS, i.e., we define

$$\left. \begin{aligned} n(t, \mathbf{x}) &= n_0 [1 + \tilde{n}(t, \mathbf{x})], \\ T(t, \mathbf{x}) &= T_H(t) [1 + \tilde{T}(t, \mathbf{x})], \\ v_i(t, \mathbf{x}) &= v_H(t) \tilde{v}_i(t, \mathbf{x}), \\ \sigma_{ij}(t, \mathbf{x}) &= \sigma_{ij}^{(H)}(t) + n_0 T_H(t) \tilde{\sigma}_{ij}(t, \mathbf{x}), \\ q_i(t, \mathbf{x}) &= q_i^{(H)}(t) + n_0 T_H(t) v_H(t) \tilde{q}_i(t, \mathbf{x}), \\ m_{ijk}(t, \mathbf{x}) &= m_{ijk}^{(H)}(t) + n_0 T_H(t) v_H(t) \tilde{m}_{ijk}(t, \mathbf{x}), \\ R_{ij}(t, \mathbf{x}) &= R_{ij}^{(H)}(t) + n_0 T_H(t) v_H(t)^2 \tilde{R}_{ij}(t, \mathbf{x}), \\ \bar{\Delta}(t, \mathbf{x}) &= \bar{\Delta}_H + \tilde{\Delta}(t, \mathbf{x}), \end{aligned} \right\} \quad (6.1)$$

where n_0 is the constant number density and $T_H(t)$ is the granular temperature in the HCS; $\bar{\Delta}_H$ is the constant solution for $\bar{\Delta}$ in the HCS; $v_H(t) = \sqrt{T_H(t)/m}$ is a reference speed in the HCS and is proportional to the adiabatic sound speed in the HCS; the reference values (HCS solutions) for all other field variables are denoted by the superscript ‘ (H) ’; the quantities with tilde denote the dimensionless perturbations in the field variables from their respective solutions in HCS. It is emphasized that $\tilde{\Delta}$ represents the perturbation in $\bar{\Delta}$ (not in Δ) from its constant value in HCS.

Inserting the field variables from (6.1) into the G26 equations (4.1)–(4.8) and (4.10), and neglecting all the nonlinear terms in perturbations, one obtains the system of linear partial differential equations in (dimensionless) perturbed variables (denoted with tilde) with time-dependent coefficients, which is given in appendix B. These equations are further simplified by exploiting the fact—concluded in § 4.2—that in the HCS, the non-equilibrium vectorial and tensorial moments— $\sigma_{ij}^{(H)}(t)$, $q_i^{(H)}(t)$, $m_{ijk}^{(H)}(t)$, $R_{ij}^{(H)}(t)$ —decay faster than the granular temperature $T_H(t)$; therefore, we drop the terms containing $\sigma_{ij}^{(H)}(t)$, $q_i^{(H)}(t)$, $m_{ijk}^{(H)}(t)$, $R_{ij}^{(H)}(t)$ in (B 1)–(B 8). Now, it is possible to convert this system of partial differential equations to a new system of partial differential equations with constant coefficients as follows. We introduce a length scale

$$L = \frac{v_H(t)}{\nu_H(t)}, \quad \text{where} \quad \nu_H(t) = \frac{16}{5} \sqrt{\pi} n_0 d^2 \sqrt{\frac{T_H(t)}{m}}, \quad (6.2)$$

to make the space variables dimensionless (i.e., $\tilde{x}_i = x_i/L$, where tilde again denotes the dimensionless space variable), and a dimensionless time \tilde{t} (see McNamara 1993) such that

$$\frac{1}{\nu_H(t)} \frac{\partial}{\partial t}(\cdot) = \frac{\partial}{\partial \tilde{t}}(\cdot). \quad (6.3)$$

This leads to

$$\tilde{t} = \nu_H(t) \tau_1 \left(1 + \frac{t}{\tau_1}\right) \ln \left(1 + \frac{t}{\tau_1}\right) \approx \nu_H(t) t + \mathcal{O}(t^2), \quad (6.4)$$

where

$$\tau_1^{-1} = \frac{5}{24}(1 - e^2) \left(1 + \frac{1}{80} \bar{\Delta}_H\right) \nu_0 \quad \text{with} \quad \nu_0 = \frac{16}{5} \sqrt{\pi} n_0 d^2 \sqrt{\frac{T_0}{m}}.$$

With these definitions of dimensionless space and time, system (B 1)–(B 8) now simplifies to

$$\frac{\partial \tilde{n}}{\partial \tilde{t}} + \frac{\partial \tilde{v}_i}{\partial \tilde{x}_i} = 0, \quad (6.5)$$

$$\frac{\partial \tilde{v}_i}{\partial \tilde{t}} + \frac{\partial \tilde{\sigma}_{ij}}{\partial \tilde{x}_j} + \frac{\partial \tilde{n}}{\partial \tilde{x}_i} + \frac{\partial \tilde{T}}{\partial \tilde{x}_i} - \frac{1}{2} \xi_0 \tilde{v}_i = 0, \quad (6.6)$$

$$\frac{\partial \tilde{T}}{\partial \tilde{t}} + \frac{2}{3} \left(\frac{\partial \tilde{q}_i}{\partial \tilde{x}_i} + \frac{\partial \tilde{v}_i}{\partial \tilde{x}_i} \right) + \xi_0 \left(\tilde{n} + \frac{1}{2} \tilde{T} \right) + \xi_1 \tilde{\Delta} = 0, \quad (6.7)$$

$$\frac{\partial \tilde{\sigma}_{ij}}{\partial \tilde{t}} + \frac{\partial \tilde{m}_{ijk}}{\partial \tilde{x}_k} + \frac{4}{5} \frac{\partial \tilde{q}_{\langle i}}{\partial \tilde{x}_{j\rangle}} + 2 \frac{\partial \tilde{v}_{\langle i}}{\partial \tilde{x}_{j\rangle}} - \xi_2 \tilde{\sigma}_{ij} + \xi_3 \tilde{R}_{ij} = 0, \quad (6.8)$$

$$\frac{\partial \tilde{q}_i}{\partial \tilde{t}} + \frac{1}{2} \frac{\partial \tilde{R}_{ij}}{\partial \tilde{x}_j} + \frac{1}{6} \frac{\partial \tilde{\Delta}}{\partial \tilde{x}_i} + \frac{1}{6} \bar{\Delta}_H \frac{\partial \tilde{n}}{\partial \tilde{x}_i} + \xi_4 \frac{\partial \tilde{T}}{\partial \tilde{x}_i} + \frac{\partial \tilde{\sigma}_{ij}}{\partial \tilde{x}_j} - \xi_5 \tilde{q}_i = 0, \quad (6.9)$$

$$\frac{\partial \tilde{m}_{ijk}}{\partial \tilde{t}} + \frac{3}{7} \frac{\partial \tilde{R}_{\langle ij}}{\partial \tilde{x}_{k\rangle}} + 3 \frac{\partial \tilde{\sigma}_{\langle ij}}{\partial \tilde{x}_{k\rangle}} - \xi_6 \tilde{m}_{ijk} = 0, \quad (6.10)$$

$$\frac{\partial \tilde{R}_{ij}}{\partial \tilde{t}} + \frac{28}{5} \frac{\partial \tilde{q}_{\langle i}}{\partial \tilde{x}_{j\rangle}} + 2 \frac{\partial \tilde{m}_{ijk}}{\partial \tilde{x}_k} + \frac{14}{15} \bar{\Delta}_H \frac{\partial \tilde{v}_{\langle i}}{\partial \tilde{x}_{j\rangle}} - \xi_7 \tilde{R}_{ij} - \xi_8 \tilde{\sigma}_{ij} = 0, \quad (6.11)$$

$$\frac{\partial \tilde{\Delta}}{\partial \tilde{t}} + \xi_9 \frac{\partial \tilde{q}_i}{\partial \tilde{x}_i} + \xi_{10} \tilde{\Delta} = 0, \quad (6.12)$$

where the coefficients

$$\xi_0 = \frac{5}{12}(1 - e^2) \left(1 + \frac{1}{80}\bar{\Delta}_H \right), \quad (6.13)$$

$$\xi_1 = \frac{1}{192}(1 - e^2), \quad (6.14)$$

$$\xi_2 = \xi_0 - \frac{1}{4}(1 + e)(3 - e) \left(1 - \frac{1}{480}\bar{\Delta}_H \right), \quad (6.15)$$

$$\xi_3 = \frac{1}{112}(1 + e)(3 - e) \left(1 + \frac{1}{160}\bar{\Delta}_H \right), \quad (6.16)$$

$$\xi_4 = \frac{5}{2} + \frac{1}{3}\bar{\Delta}_H, \quad (6.17)$$

$$\xi_5 = \frac{3}{2}\xi_0 - \frac{1}{48}(1 + e) \left[(49 - 33e) + \frac{(19 - 3e)}{480}\bar{\Delta}_H \right], \quad (6.18)$$

$$\xi_6 = \frac{3}{2} \left[\xi_0 - \frac{1}{4}(1 + e)(3 - e) \left(1 - \frac{1}{1120}\bar{\Delta}_H \right) \right], \quad (6.19)$$

$$\xi_7 = 2\xi_0 - \frac{1}{336}(1 + e) \left[(436 - 267e + 66e^2 - 30e^3) - \frac{(52 - 27e + 66e^2 - 30e^3)}{480}\bar{\Delta}_H \right], \quad (6.20)$$

$$\xi_8 = \frac{1}{12}(1 + e) \left[(11 - 2e - 22e^2 + 10e^3) + \frac{(202 - 207e - 66e^2 + 30e^3)}{480}\bar{\Delta}_H \right], \quad (6.21)$$

$$\xi_9 = 8 - \frac{4}{3}\bar{\Delta}_H, \quad (6.22)$$

$$\xi_{10} = \frac{1}{192}(1 + e) \left[(81 - 17e + 30e^2 - 30e^3) - 4(1 - e)\bar{\Delta}_H \right] \quad (6.23)$$

depend only on the parameter e , the coefficient of restitution. It is noteworthy to point out that we take

$$\bar{\Delta}_H = 15 a_2 = \frac{240(1 - e)(1 - 2e^2)}{81 - 17e + 30e^2 - 30e^3} \quad (6.24)$$

as given in (4.26), since we have seen in §4 that the nonlinear terms of scalar moments as well as the higher-order scalar moments do not affect the solutions in HCS significantly.

Now, we assume a normal mode solution of the form

$$(\tilde{n}, \tilde{v}_i, \tilde{T}, \tilde{\sigma}_{ij}, \tilde{q}_i, \tilde{m}_{ijk}, \tilde{R}_{ij}, \tilde{\Delta})^\top = (\hat{n}, \hat{v}_i, \hat{T}, \hat{\sigma}_{ij}, \hat{q}_i, \hat{m}_{ijk}, \hat{R}_{ij}, \hat{\Delta})^\top \exp[\mathfrak{i}(\mathbf{k} \cdot \tilde{\mathbf{x}} - \omega \tilde{t})] \quad (6.25)$$

for system (6.5)–(6.12). Here, quantities with hats denote the complex amplitudes of the perturbed field variables; \mathfrak{i} is imaginary unit; \mathbf{k} and ω are the (dimensionless) wavevector and (dimensionless) frequency, respectively, of the disturbance. For the temporal stability analysis—to be analyzed here—the wavevector \mathbf{k} is assumed to be real and the frequency ω is assumed to be complex. The real part of complex frequency, $\text{Re}(\omega)$, determines the phase velocity $\mathbf{v}_{\text{ph}} = \text{Re}(\omega)/\mathbf{k}$ of the corresponding wave whereas the imaginary part of complex frequency, $\text{Im}(\omega)$, determines whether the amplitude of the disturbance grows or decays in time. From the normal mode solution (6.25), it is clear that the solution will decay (or grow) in time if the imaginary part of complex frequency is non-positive (or positive). Consequently, stability of the system requires the imaginary part of frequency to be non-positive, i.e., $\text{Im}(\omega) \leq 0$.

If we assume that the wavevector of the disturbance is parallel to the x -axis, i.e.,

$\mathbf{k} = k \hat{\mathbf{x}}$ where the wavenumber k is the magnitude of the wavevector \mathbf{k} and $\hat{\mathbf{x}}$ is the unit vector in x -direction, we get two independent eigenvalue problems—namely, the longitudinal problem and the transverse problem—for the amplitude of the disturbance in two dimensions. These problems read

$$\mathcal{A} \begin{bmatrix} \hat{n} \\ \hat{v}_x \\ \hat{T} \\ \hat{\sigma}_{xx} \\ \hat{q}_x \\ \hat{m}_{xxx} \\ \hat{R}_{xx} \\ \hat{\Delta} \end{bmatrix} = \begin{bmatrix} 0 \\ 0 \\ 0 \\ 0 \\ 0 \\ 0 \\ 0 \\ 0 \end{bmatrix} \quad \text{and} \quad \mathcal{B} \begin{bmatrix} \hat{v}_y \\ \hat{\sigma}_{xy} \\ \hat{q}_y \\ \hat{m}_{xxy} \\ \hat{R}_{xy} \end{bmatrix} = \begin{bmatrix} 0 \\ 0 \\ 0 \\ 0 \\ 0 \end{bmatrix} \quad (6.26)$$

respectively, where

$$\mathcal{A} = \begin{bmatrix} \omega & -k & 0 & 0 & 0 & 0 & 0 & 0 \\ -k & \omega - \mathbf{i}\frac{\xi_0}{2} & -k & -k & 0 & 0 & 0 & 0 \\ \mathbf{i}\xi_0 & -\frac{2k}{3} & \omega + \mathbf{i}\frac{\xi_0}{2} & 0 & -\frac{2k}{3} & 0 & 0 & \mathbf{i}\xi_1 \\ 0 & -\frac{4k}{3} & 0 & \omega - \mathbf{i}\xi_2 & -\frac{8k}{15} & -k & \mathbf{i}\xi_3 & 0 \\ -\frac{k\bar{\Delta}_H}{6} & 0 & -k\xi_4 & -k & \omega - \mathbf{i}\xi_5 & 0 & -\frac{k}{2} & -\frac{k}{6} \\ 0 & 0 & 0 & -\frac{9k}{5} & 0 & \omega - \mathbf{i}\xi_6 & -\frac{9k}{35} & 0 \\ 0 & -\frac{28k\bar{\Delta}_H}{45} & 0 & -\mathbf{i}\xi_8 & -\frac{56k}{15} & -2k & \omega - \mathbf{i}\xi_7 & 0 \\ 0 & 0 & 0 & 0 & -k\xi_9 & 0 & 0 & \omega + \mathbf{i}\xi_{10} \end{bmatrix}, \quad (6.27)$$

and

$$\mathcal{B} = \begin{bmatrix} \omega - \mathbf{i}\frac{\xi_0}{2} & -k & 0 & 0 & 0 \\ -k & \omega - \mathbf{i}\xi_2 & -\frac{2k}{5} & -k & \mathbf{i}\xi_3 \\ 0 & -k & \omega - \mathbf{i}\xi_5 & 0 & -\frac{k}{2} \\ 0 & -\frac{3k}{5} & 0 & \omega - \mathbf{i}\xi_6 & -\frac{3k}{35} \\ -\frac{7k\bar{\Delta}_H}{15} & -\mathbf{i}\xi_8 & -\frac{14k}{5} & -2k & \omega - \mathbf{i}\xi_7 \end{bmatrix}. \quad (6.28)$$

For nontrivial solution of each eigenvalue problem in (6.26), the determinant of each of the two matrices \mathcal{A} and \mathcal{B} must vanish, i.e., $\det(\mathcal{A}) = 0$ and $\det(\mathcal{B}) = 0$. The vanishing condition of the determinant of matrix \mathcal{A} (or \mathcal{B}) leads to the dispersion relation—a relation between the wavenumber k and frequency ω , which is usually exploited to express ω as a function of k or vice versa—for the longitudinal (or transverse) problem. As we are interested in the temporal stability analysis, we assume that the wavenumber k is real and solve the equations $\det(\mathcal{A}) = 0$ and $\det(\mathcal{B}) = 0$ in order to express the frequency as $\omega \equiv \omega(k)$.

6.1. Eigenmodes

The condition $\det(\mathcal{A}) = 0$ results into eight eigenmodes for the longitudinal system (6.26)₁. These eigenmodes for the coefficient of restitution $e = 0.75$ and $e = 1$ are shown in figures 6 and 7, respectively. The left panels in each of figures 6 and 7 depict the real part of frequency, $\text{Re}(\omega)$, while the right panels display the imaginary part of frequency, $\text{Im}(\omega)$, all plotted over the wavenumber k . For very small wavenumbers ($k \lesssim 0.02$), all the eigenmodes of the longitudinal system (6.26)₁ are stationary in case of $e = 0.75$ (see the left panel of figure 6); however, as the wavenumber starts increasing, a pair of traveling modes commences at $k \approx 0.02$, another pair of slow traveling modes commences

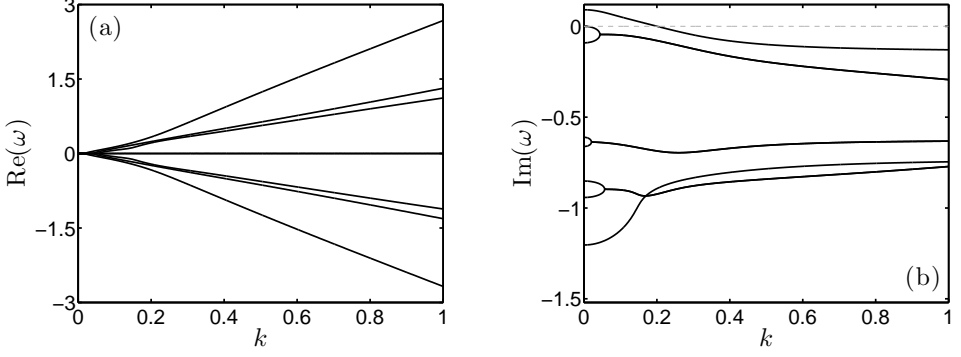


FIGURE 6. Eigenmodes from the longitudinal system (6.26)₁ for the coefficient of restitution $e = 0.75$: (a) real part of the frequency ω and (b) imaginary part of the frequency ω representing the growth (or decay) rate.

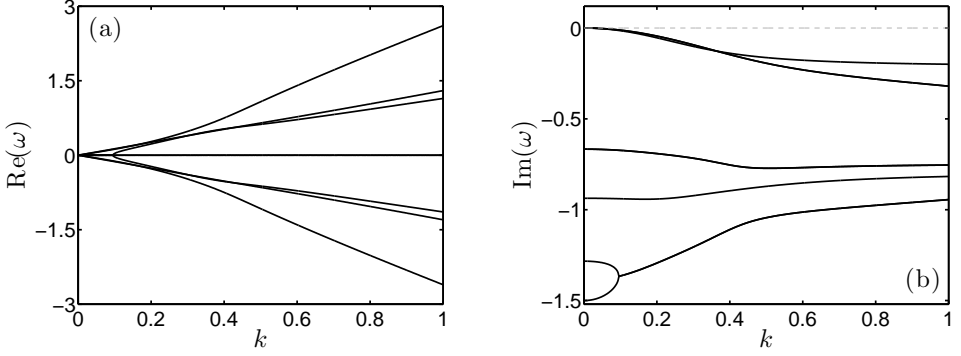


FIGURE 7. Same as figure 6 but in the elastic case, i.e., for the coefficient of restitution $e = 1$.

at $k \approx 0.043$ and a third pair of even slower traveling modes starts at $k \approx 0.056$. Each pair of traveling eigenmodes propagates in the opposite directions since the corresponding eigenvalues are in complex conjugate pairs. The remaining two eigenmodes continue to be stationary for all wavenumbers since the frequencies associated with them are purely imaginary. In the elastic case, i.e. for $e = 1$ (see the left panel of figure 7), there are also two eigenmodes which remain stationary for all wavenumbers and three pairs of traveling eigenmodes. However, two pairs of traveling eigenmodes commence propagating in the opposite directions at $k = 0$ itself. These two pairs of eigenmodes travel with the same speeds for $0 \leq k \lesssim 0.19$ whereas for $k \gtrsim 0.19$ one pair of eigenmodes travels faster than the other. It may also be interesting to note that out of these two pairs of eigenmodes, the speed of the one pair traveling with slower speed coincides with the speed of a third pair of traveling eigenmodes—which starts propagating at $k \approx 0.095$ in the opposite directions with even slower speed—for $0.27 \lesssim k \lesssim 0.45$. It can also be noticed by comparing the left panels of figures 6 and 7 that the speeds of traveling eigenmodes in case of $e = 0.75$ (figure 6) are almost same as those of corresponding traveling eigenmodes in elastic case (figure 7) for wavenumbers $k \gtrsim 0.7$.

Since the complex eigenvalues of a matrix occur in pairs, the imaginary parts of frequencies, $\text{Im}(\omega)$, of a pair of traveling eigenmodes coincide beyond the wavenumber at which they start propagating. This is clearly reflected in right panels of figures 6 and 7: the imaginary parts of frequencies, $\text{Im}(\omega)$, of the three pairs of traveling waves—in the left panels (i) starting at $k \approx 0.02$, $k \approx 0.043$ and $k \approx 0.056$ in case of $e = 0.75$ (figure 6)

and (ii) two pairs starting at $k = 0$ and one starting at $k \approx 0.095$ in the elastic case (figure 7)—merge together beyond these wavenumber values (compare the corresponding left and right panels of figures 6 and 7). As we have discussed above that the imaginary part of frequency, $\text{Im}(\omega)$, is solely responsible for the stability of the solution: stable if $\text{Im}(\omega) \leq 0$ and unstable if $\text{Im}(\omega) > 0$, it is clear from the right panel of figure 6 that one eigenmode (for which $\text{Im}(\omega) > 0$) of the longitudinal system (6.26)₁ in case of $e = 0.75$ is unstable whereas all other eigenmodes are stable for all wavenumbers. On the other hand, it is evident from the right panel of figure 7 that for the elastic case (i.e., $e = 1$) all the eigenmodes of the longitudinal system (6.26)₁ are stable for all wavenumbers. The unstable eigenmode in case of $e = 0.75$ turns stable beyond $k \approx 0.2005$ (see the right panel of figure 6) since beyond this value of the wavenumber, $\text{Im}(\omega)$ becomes negative. A value of wavenumber k at which the imaginary part of frequency, $\text{Im}(\omega)$, switches its sign is referred to as the *critical* wavenumber. In other words, the corresponding eigenmode is unstable (or stable) for the wavenumbers below the critical wavenumber since $\text{Im}(\omega) > 0$ (or $\text{Im}(\omega) \leq 0$) for them while it is stable (or unstable) for those above the critical wavenumber since $\text{Im}(\omega) \leq 0$ (or $\text{Im}(\omega) > 0$) for them. Thus, $k \approx 0.2005$ is the critical wavenumber for the longitudinal system (6.26)₁ in case of $e = 0.75$.

The condition $\det(\mathcal{B}) = 0$ leads to five eigenmodes for the transverse system (6.26)₂. These eigenmodes for the coefficient of restitution $e = 0.75$ and $e = 1$ are illustrated in figures 8 and 9, respectively. The left panels in each of figures 8 and 9 again delineate the real part of frequency, $\text{Re}(\omega)$, while the right panels portray the imaginary part of frequency, $\text{Im}(\omega)$, all plotted over the wavenumber k . For very small wavenumbers ($k \lesssim 0.065$), all the eigenmodes of the transverse system (6.26)₂ are stationary in case of $e = 0.75$ (see the left panel of figure 8). A pair of traveling modes commences at $k \approx 0.065$ and another pair of slow traveling modes commences at $k \approx 0.562$. Each pair of traveling eigenmodes propagates in the opposite directions, and one remaining eigenmode continue to be stationary for all wavenumbers since the frequency associated with it is purely imaginary. For the same reason as discussed above, the imaginary parts of frequencies of each pair of traveling eigenmodes coincide beyond the wavenumbers at which they start propagating (one pair coincides for $k \gtrsim 0.065$ and another for $k \gtrsim 0.562$ in the right panel of figure 8). Furthermore, it is noted from the right panel of figure 8 that one eigenmode of the transverse system (6.26)₂ in case of $e = 0.75$ is also unstable for wavenumber values below the critical wavenumber which is $k \approx 0.2827$ while it is stable for wavenumber values above the critical wavenumber; the remaining four eigenmodes are always stable for all values of wavenumber k .

In the elastic case, for $e = 1$ (figure 9), all the eigenmodes of the transverse system (6.26)₂ are stationary for small wavenumbers ($k \lesssim 0.23$). A pair of traveling eigenmodes commences at $k \approx 0.23$ but turns back to become stationary on slight increase in the wavenumber (at $k \approx 0.241$), refer to the zoomed region shown in the insets of figure 9. On further increase in the wavenumber, a pair of traveling modes starts at $k \approx 0.25$ and another pair of slow traveling modes commences at $k \approx 0.574$. Each pair of traveling eigenmodes propagates in the opposite directions, and one eigenmode remains stationary for all wavenumbers since the frequency associated with it is purely imaginary. For the same reason as discussed above, the imaginary parts of frequencies of each pair of traveling eigenmodes coincide for the wavenumbers for which they are propagating—one pair coincides for $0.23 \lesssim k \lesssim 0.241$ (see the inset in the right panel of figure 9), one pair for $k \gtrsim 0.25$ and another for $k \gtrsim 0.574$ in the right panel of figure 9). Furthermore, it is noted from the right panel of figure 9 that all five eigenmodes of the transverse system (6.26)₂ are always stable in the elastic case. It can again be noticed from the left panels of figures 8 and 9 that the speeds of traveling eigenmodes in case of $e = 0.75$ (figure 8)

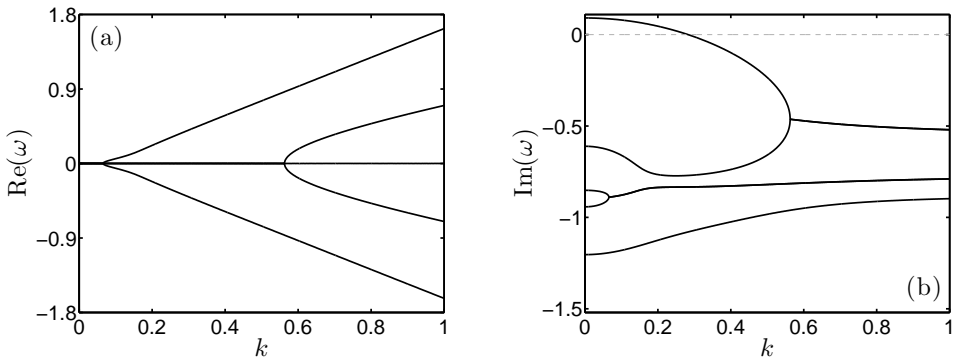


FIGURE 8. Eigenmodes from the transverse system (6.26)₂ for the coefficient of restitution $e = 0.75$: (a) real part of the frequency ω and (b) imaginary part of the frequency ω representing the growth or decay rate.

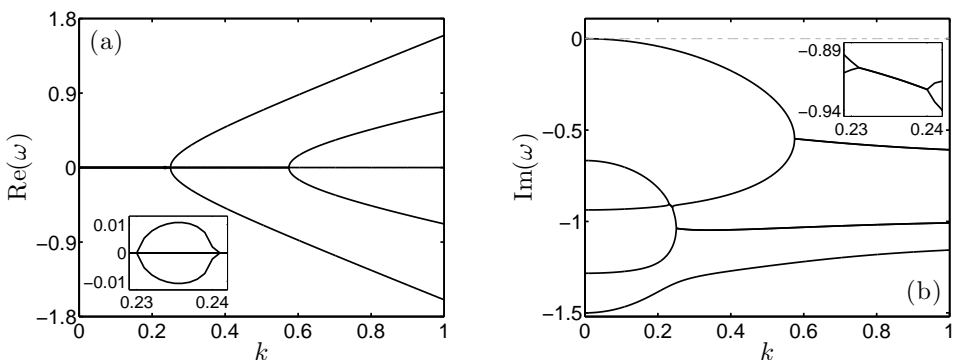


FIGURE 9. Same as figure 8 but in the elastic case, i.e., for the coefficient of restitution $e = 1$. The insets exhibit the zoomed region where a pair of stationary eigenmodes changes to a pair of traveling eigenmodes with increasing wavenumber and turns back to become stationary with further increase in the wavenumber.

are almost same as those of corresponding traveling eigenmodes in elastic case (figure 9) for wavenumbers $k \gtrsim 0.6$.

6.2. Eigenmodes in small wavenumber limit

There is another interesting classification of eigenmodes in the small wavenumber limit (or long wavelength limit), i.e. in the limit $k \rightarrow 0$: an eigenmode is referred to as a *hydrodynamic* mode if the frequency $\omega(k)$ of this eigenmode vanishes in the limit $k \rightarrow 0$ while it is referred to as a *kinetic* mode if its frequency $\omega(k)$ attains a nonzero constant value in the limit $k \rightarrow 0$ (Kremer & Marques Jr. 2011). In order to explore the behavior of the eigenmodes in the small wavenumber limit (i.e., in the limit $k \rightarrow 0$), the frequency ω is expressed in powers of k (see Kremer & Marques Jr. 2011):

$$\omega = \gamma_0 + \gamma_1 k + \gamma_2 k^2 + \dots \quad (6.29)$$

The unknown coefficients $\gamma_0, \gamma_1, \gamma_2, \dots$ in the above expansion are determined by inserting expansion (6.29) for ω into the vanishing determinant conditions $\det(\mathcal{A}) = 0$ (or $\det(\mathcal{B}) = 0$), and solving the algebraic equations resulting from the comparison of coefficients of each power of k on both sides of the equation. With this technique, it turns out that in the limit $k \rightarrow 0$, the frequencies of eight eigenmodes of the longitudinal

system (6.26)₁ in the inelastic (i.e., $e \neq 1$) case are related to the wavenumber k via

$$\left. \begin{aligned} \omega^{(1)} &= -\frac{2\mathfrak{i}}{\xi_0}k^2 + \dots \\ \omega^{(2)} &= -\frac{\mathfrak{i}\xi_0}{2} + \frac{4\mathfrak{i}}{3} \left[\frac{2}{\xi_0} + \frac{\xi_4}{(\xi_0 + 2\xi_5)} \left\{ 1 + \frac{3\xi_1\xi_9}{(\xi_0 - 2\xi_{10})} \right\} \right] k^2 + \dots \\ \omega^{(3)} &= \frac{\mathfrak{i}\xi_0}{2} - \frac{2\mathfrak{i}}{3} \left[\frac{1}{\xi_0} + \frac{4}{15} \left\{ \frac{14\bar{\Delta}_H\xi_3 - 15(\xi_0 - 2\xi_7)}{(\xi_0 - 2\xi_2)(\xi_0 - 2\xi_7) + 4\xi_3\xi_8} \right\} \right] k^2 + \dots \\ \omega^{(4)} &= -\mathfrak{i}\xi_{10} + \frac{\mathfrak{i}}{6} \frac{\xi_9}{(\xi_5 + \xi_{10})} \left(1 - \frac{12\xi_1\xi_4}{\xi_0 - 2\xi_{10}} \right) k^2 + \dots \\ \omega^{(5)} &= \mathfrak{i}\xi_5 - \frac{4\mathfrak{i}}{3}\vartheta k^2 + \dots \\ \omega^{(6)} &= \mathfrak{i}\xi_6 - \frac{9\mathfrak{i}}{35} \left[\frac{2\xi_2 + 14\xi_3 - 9\xi_6 + 7\xi_7 - \xi_8}{(\xi_2 - \xi_6)(\xi_6 - \xi_7) - \xi_3\xi_8} \right] k^2 + \dots \\ \omega^{(7)} &= \frac{\mathfrak{i}\xi_-}{2} + \frac{\mathfrak{i}}{630} \left(\frac{\vartheta_1 + \vartheta_2\xi_-}{\vartheta_0} \right) k^2 + \dots \\ \omega^{(8)} &= \frac{\mathfrak{i}\xi_+}{2} + \frac{\mathfrak{i}}{630} \left(\frac{\vartheta_1 + \vartheta_2\xi_+}{\vartheta_0} \right) k^2 + \dots, \end{aligned} \right\} \quad (6.30)$$

and those in the elastic (i.e., $e = 1$) case are related to the wavenumber k via

$$\left. \begin{aligned} \omega^{(1)} &= -\frac{3\mathfrak{i}}{2}k^2 + \dots \\ \omega^{(2)} &= -\sqrt{\frac{5}{3}}k - \frac{713\mathfrak{i}}{606}k^2 + \dots \\ \omega^{(3)} &= \sqrt{\frac{5}{3}}k - \frac{713\mathfrak{i}}{606}k^2 + \dots \\ \omega^{(4)} &= -\frac{2\mathfrak{i}}{3} - \frac{2}{\sqrt{3}}k - \frac{59\mathfrak{i}}{84}k^2 + \dots \\ \omega^{(5)} &= -\frac{2\mathfrak{i}}{3} + \frac{2}{\sqrt{3}}k - \frac{59\mathfrak{i}}{84}k^2 + \dots \\ \omega^{(6)} &= -\frac{3\mathfrak{i}}{2} + \frac{342\mathfrak{i}}{41}k^2 + \dots \\ \omega^{(7)} &= -\frac{(373 - \sqrt{3385})\mathfrak{i}}{336} - \frac{(453843875 - 6402969\sqrt{3385})\mathfrak{i}}{294362985}k^2 + \dots \\ \omega^{(8)} &= -\frac{(373 + \sqrt{3385})\mathfrak{i}}{336} - \frac{(453843875 + 6402969\sqrt{3385})\mathfrak{i}}{294362985}k^2 + \dots \end{aligned} \right\} \quad (6.31)$$

The unknown constants ξ_- , ξ_+ , ϑ and ϑ_0 in (6.30) are given by

$$\begin{aligned} \xi_- &= \xi_2 + \xi_7 - \mathfrak{i}\sqrt{4\xi_3\xi_8 - (\xi_2 - \xi_7)^2}, \\ \xi_+ &= \xi_2 + \xi_7 + \mathfrak{i}\sqrt{4\xi_3\xi_8 - (\xi_2 - \xi_7)^2}, \\ \vartheta &= \frac{1}{8} \frac{\xi_9}{(\xi_5 + \xi_{10})} + \frac{\xi_4}{(\xi_0 + 2\xi_5)} \left[1 - \frac{3}{2} \frac{\xi_1\xi_9}{(\xi_5 + \xi_{10})} \right] + \frac{1}{5} \left[\frac{7\xi_2 + 14\xi_3 - 9\xi_5 + 2\xi_7 - \xi_8}{(\xi_2 - \xi_5)(\xi_5 - \xi_7) - \xi_3\xi_8} \right], \\ \vartheta_0 &= [(\xi_2 - \xi_7)^2 - 4\xi_3\xi_8][(\xi_2 - \xi_5)(\xi_5 - \xi_7) - \xi_3\xi_8][(\xi_2 - \xi_6)(\xi_6 - \xi_7) - \xi_3\xi_8] \\ &\quad \times [(\xi_0 - 2\xi_2)(\xi_0 - 2\xi_7) + 4\xi_3\xi_8]; \end{aligned}$$

the constants ϑ_1 and ϑ_2 in (6.30) are too cumbersome to write here.

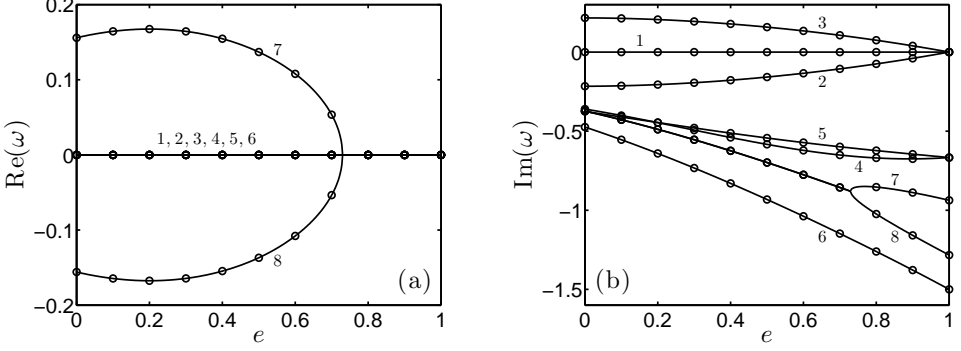


FIGURE 10. Real and imaginary parts of frequencies associated with the eigenmodes of the longitudinal system $(6.26)_1$ plotted over the coefficient of restitution e for wavenumber $k = 0$. The lines denote the frequencies obtained directly from the condition $\det(\mathcal{A}) = 0$ on substituting $k = 0$ in the matrix \mathcal{A} while the circles denote the frequencies obtained from the analytic expressions (6.30) and (6.31) in the limit $k \rightarrow 0$. The numbers represent the numbering of eigenmodes as given in (6.30) and (6.31).

It is clear from (6.30) that, in the limiting case of limit $k \rightarrow 0$, out of eight eigenmodes of the longitudinal system $(6.26)_1$, one mode is hydrodynamic while the rest seven modes are kinetic in the inelastic case (i.e., $e \neq 1$); however, from (6.31), it is evident that three modes out of eight eigenmodes of the longitudinal system $(6.26)_1$ are hydrodynamic in the elastic case while only the remaining five modes are kinetic. Figure 10 illustrates the real (in the left panel) and imaginary (in the right panel) parts of frequencies ω —associated with the eigenmodes of the longitudinal system $(6.26)_1$ —plotted over the coefficient of restitution e for $k = 0$. The solid lines in figure 10 denote the frequencies obtained directly from the condition $\det(\mathcal{A}) = 0$ on substituting $k = 0$ in the matrix \mathcal{A} while the circles denote the frequencies obtained from the analytic expressions (6.30) and (6.31) in the limit $k \rightarrow 0$; moreover, the numbers in figure 10 represent the numbering of eigenmodes as given in (6.30) and (6.31). From the right panel of figure 10, one may notice that the magnitude of imaginary part of frequency, $\text{Im}(\omega)$, for eigenmodes 2 and 3 decrease as the coefficient of restitution increases and they vanish for $e = 1$; thus, it is concluded that the longitudinal system $(6.26)_1$ has three hydrodynamic modes exclusively for the elastic case ($e = 1$); in the inelastic case ($e \neq 1$), the longitudinal system $(6.26)_1$ always has only a single hydrodynamic mode. The left panel of figure 10 shows that for the wavenumber $k = 0$ only two eigenmodes (7 and 8) have nonzero real part of frequency for the coefficient of restitution $0 \leq e \lesssim 0.73$ while the rest six eigenmodes (1, 2, ..., 6) are purely diffusive since the frequencies associated with them are purely imaginary. This can also be seen from (6.30): apart from frequency $\omega^{(1)}$ which is zero in the limit $k \rightarrow 0$ for all e , the frequencies $\omega^{(2)}, \omega^{(3)}, \dots, \omega^{(6)}$ are purely imaginary in the limit $k \rightarrow 0$; the frequencies $\omega^{(7)}$ and $\omega^{(8)}$ are, in general, complex with nonzero real part—even in the limit $k \rightarrow 0$ —since ξ_- and ξ_+ may be complex depending on the value of the coefficient of restitution; nonetheless, in the limit $k \rightarrow 0$, $\omega^{(7)}$ and $\omega^{(8)}$ also become purely imaginary for $0.73 \lesssim e \leq 1$ —it can be seen from (6.31) for $e = 1$ as well as in the left panel of figure 10. One can further perceive from the right panel of figure 10 that the imaginary part of frequency of one eigenmode (denoted by number ‘3’) is always positive for $e \neq 1$; consequently, one eigenmode of longitudinal system $(6.26)_1$ in the inelastic case ($e \neq 1$) is unstable in the limit $k \rightarrow 0$ whereas all the other eigenmodes are stable in this limit. Nevertheless, all the eigenmodes of longitudinal system $(6.26)_1$ in the elastic case ($e = 1$) are always stable for any wavenumber (see also the right panel of figure 7).

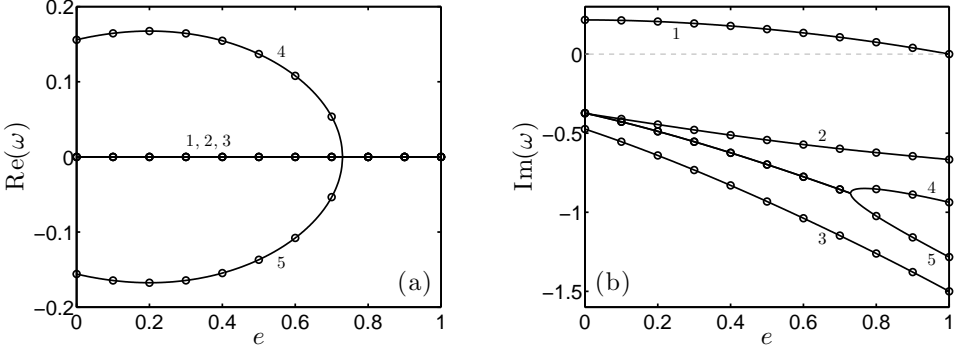


FIGURE 11. Same as figure 10 but for the transverse system $(6.26)_2$. The lines denote the frequencies obtained directly from the condition $\det(\mathcal{B}) = 0$ on substituting $k = 0$ in the matrix \mathcal{B} while the circles denote the frequencies obtained from the analytic expressions (6.32) and (6.33) in the limit $k \rightarrow 0$. The numbers represent the numbering of eigenmodes as given in (6.32) and (6.33).

By the similar frequency expansion technique employed above, the frequencies of five eigenmodes of the transverse system $(6.26)_2$ in the limit $k \rightarrow 0$ are related to the wavenumber k via

$$\left. \begin{aligned} \omega^{(1)} &= \frac{i\xi_0}{2} + \frac{2i}{15} \left[\frac{14\bar{\Delta}_H\xi_3 - 15(\xi_0 - 2\xi_7)}{(\xi_0 - 2\xi_2)(\xi_0 - 2\xi_7) + 4\xi_3\xi_8} \right] k^2 + \dots \\ \omega^{(2)} &= i\xi_5 - \frac{i}{5} \left[\frac{7\xi_2 + 14\xi_3 - 9\xi_5 + 2\xi_7 - \xi_8}{(\xi_2 - \xi_5)(\xi_5 - \xi_7) - \xi_3\xi_8} \right] k^2 + \dots \\ \omega^{(3)} &= i\xi_6 - \frac{3i}{35} \left[\frac{2\xi_2 + 14\xi_3 - 9\xi_6 + 7\xi_7 - \xi_8}{(\xi_2 - \xi_6)(\xi_6 - \xi_7) - \xi_3\xi_8} \right] k^2 + \dots \\ \omega^{(4)} &= \frac{i\xi_-}{2} + \frac{i}{210} \left(\frac{\vartheta_3 + \vartheta_4\xi_-}{\vartheta_0} \right) k^2 + \dots \\ \omega^{(5)} &= \frac{i\xi_+}{2} + \frac{i}{210} \left(\frac{\vartheta_3 + \vartheta_4\xi_+}{\vartheta_0} \right) k^2 + \dots \end{aligned} \right\} \quad (6.32)$$

and, in the elastic ($e = 1$) case, they simplify to

$$\left. \begin{aligned} \omega^{(1)} &= -\frac{205i}{202}k^2 + \dots \\ \omega^{(2)} &= -\frac{2i}{3} - \frac{41i}{14}k^2 + \dots \\ \omega^{(3)} &= -\frac{3i}{2} + \frac{114i}{41}k^2 + \dots \\ \omega^{(4)} &= -\frac{(373 - \sqrt{3385})i}{336} + \frac{5(2282167 - 12093\sqrt{3385})i}{19624199}k^2 + \dots \\ \omega^{(5)} &= -\frac{(373 + \sqrt{3385})i}{336} + \frac{5(2282167 + 12093\sqrt{3385})i}{19624199}k^2 + \dots \end{aligned} \right\} \quad (6.33)$$

The constants ϑ_3 and ϑ_4 in (6.32) are also too cumbersome to write here.

Expressions (6.32) and (6.33) suggest that, in the limiting case of limit $k \rightarrow 0$, all five eigenmodes of the transverse system $(6.26)_2$ are kinetic for all values of the coefficient of restitution e except in the elastic case (i.e., for $e = 1$) for which $\xi_0 = 0$ and consequently, one of the five eigenmodes is hydrodynamic in the elastic limit. Figure 11 illustrates

the real (in the left panel) and imaginary (in the right panel) parts of frequencies ω —associated with the eigenmodes of the transverse system (6.26)₂—plotted over the coefficient of restitution e for $k = 0$. The solid lines in figure 11 denote the frequencies obtained directly from the condition $\det(\mathcal{B}) = 0$ on substituting $k = 0$ in the matrix \mathcal{B} while the circles denote the frequencies obtained from the analytic expressions (6.32) and (6.33) in the limit $k \rightarrow 0$; moreover, the numbers in figure 11 represent the numbering of eigenmodes as given in (6.32). From the right panel of figure 11, one may notice that the imaginary part of frequency, $\text{Im}(\omega)$, for one eigenmode (denoted by ‘1’) is non-negative and decreases as the coefficient of restitution increases and, finally, vanishes for $e = 1$; therefore, it is concluded that one eigenmode (denoted by ‘1’) of the transverse system (6.26)₂ in the elastic case (i.e., for $e = 1$) is hydrodynamic since its real and imaginary parts are zero (cf. (6.33)₁) and that this mode of the transverse system (6.26)₂ in the inelastic case ($e \neq 1$) is unstable in the limit $k \rightarrow 0$ whereas all the other eigenmodes are stable in this limit. Nonetheless, all the eigenmodes of transverse system (6.26)₂ in the elastic case ($e = 1$) are always stable for any wavenumber (see also the right panel of figure 9). The left panel of figure 11 shows that for the wavenumber $k = 0$ only two eigenmodes (4 and 5) have nonzero real part of frequency for the coefficient of restitution $0 \leq e \lesssim 0.73$ while the remaining three eigenmodes (1, 2 and 3) are purely diffusive since the frequencies associated with them are purely imaginary. This can also be seen from (6.32): the frequencies $\omega^{(1)}, \omega^{(2)}$ and $\omega^{(3)}$ are purely imaginary in the limit $k \rightarrow 0$; the frequencies $\omega^{(4)}$ and $\omega^{(5)}$ are, in general, complex with nonzero real part—even in the limit $k \rightarrow 0$ —since ξ_- and ξ_+ may be complex depending on the value of the coefficient of restitution; nonetheless, in the limit $k \rightarrow 0$, $\omega^{(4)}$ and $\omega^{(5)}$ also become purely imaginary for $0.73 \lesssim e \leq 1$ —it can be seen from (6.33) for $e = 1$ as well as in the left panel of figure 11.

6.3. Comparison among various Grad moment theories

As discussed in § 3.3, one can obtain a lower-level system of Grad moment equations by dropping the appropriate field variables in the system of G26 equations. In the same way, one can obtain the longitudinal and transverse systems associated with the G13, G14, G20 and G21 equations by dropping the appropriate variables and corresponding rows and columns of the matrices \mathcal{A} and \mathcal{B} in (6.26). Note that the transverse systems for the G13 and G14 equations are same since the field variable $\hat{\Delta}$ does not appear in the list of unknowns of the transverse system (see (6.26)₂); for the same reason, the transverse systems for the G20 and G21 equations are also same. It is also important to note that the results for the G13 theory presented below are equivalent to those of Kremer & Marques Jr. (2011) since they assumed a constant HCS value for the field variable $\hat{\Delta}$ and studied the eigenmodes of the G13 theory essentially.

We have seen above that one eigenmode of both the longitudinal and transverse systems associated with the G26 equations—in the inelastic ($e \neq 1$) case—is unstable below some critical wavenumber values (see the right panels of figures 6 and 8). Here, we investigate the imaginary part of frequency of the least stable eigenmode for different values of wavenumber and all possible values of the coefficient of restitution. Figures 12 and 13 illustrate the zero contours of the least stable eigenmode of the (a) longitudinal and (b) transverse systems associated with the G13 and G26 equations, respectively in (e, k) -plane. The black solid line represents the critical wavenumber below which the system is unstable (region depicted with gray color) and above which the system is stable (region shown with white color). The left panels of figures 12 and 13 unveil that the longitudinal system associated with the G13 equations is unstable for $0 \leq e \lesssim 0.21$ and for $0 \leq k \leq 1$ (in fact, for any wavenumber apparently) whereas that associated with

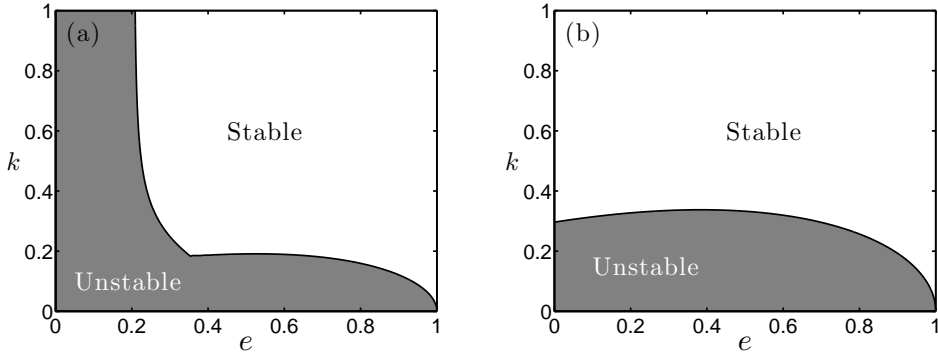


FIGURE 12. Stability diagram in (e, k) -plane showing the unstable (in gray color) and stable (in white color) regions for (a) longitudinal and (b) transverse systems associated with G13 theory.

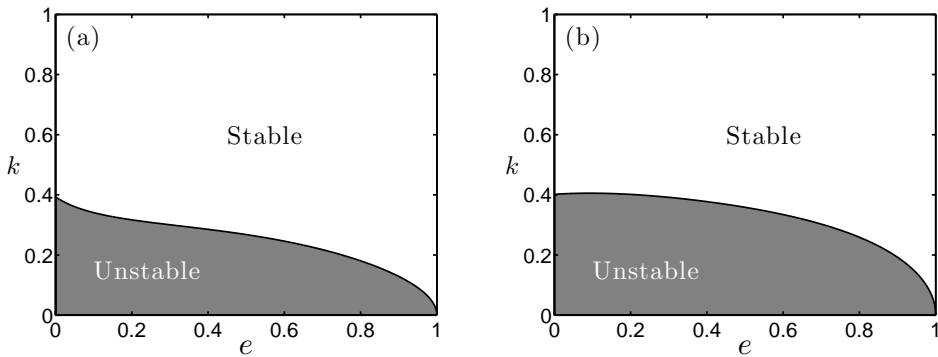


FIGURE 13. Stability diagram in (e, k) -plane showing the unstable (in gray color) and stable (in white color) regions for (a) longitudinal and (b) transverse systems associated with G26 theory.

the G26 equations is stable above some critical wavenumber for all values of e . Thus, the G13 theory of [Kremer & Marques Jr. \(2011\)](#) may not be suitable to the granular flows having coefficient of restitution $e \lesssim 0.35$ (the point where the critical wavenumber from the G13 theory attains a sudden jump). The critical wavenumber in the transverse system associated with the G13 equations (right panel of figure 12)—for small values of coefficient of restitution ($0 \leq e \lesssim 0.4$)—increases with increasing e , however, that in the transverse system associated with the G26 equations (right panel of figure 13) decreases with increasing e in the same region. Moreover, the instability region is more in the transverse system associated with the G26 equations than that in the transverse system associated with the G13 equations (cf. the right panels of figures 12 and 13). We have also found (but not shown here) that the unstable eigenmodes in both the longitudinal and transverse systems belong to stationary waves, i.e., the real parts of their frequencies are zero, and consequently, instabilities in both the systems are stationary.

In order to compare the critical wavenumbers for the longitudinal and transverse systems associated with various moment theories (G13, G14, G20, G21 and G26), we again plot the zero contours of the least stable eigenmode of the (a) longitudinal and (b) transverse systems associated with these moment theories in (e, k) -plane in figure 14. Recall that the transverse systems for the G13 and G14 equations are same and those for the G20 and G21 equations are also same. Therefore, the curves representing the G14 (in red color) and G21 (in black color) theories in right panel of figure 14 also represent the G13 and G20 theories, respectively. Apparently, all moment theories predict same

critical wavenumber for the longitudinal system when $0.94 \lesssim e \leq 1$ (see the left panel of figure 14) and same critical wavenumber for the transverse system when $0.75 \lesssim e \leq 1$ (see the right panel of figure 14). From the right panel of figure 14, we see that for the transverse system, the critical wavenumber profiles predicted by all Grad moment theories are qualitatively similar except for that in the region where $0 \leq e \lesssim 0.4$; in this region, the critical wavenumber predicted by the G14 equations increases with increasing e while that predicted by the G21 equations remains more or less constant and that predicted by the G26 equations decreases with increasing e . Also, the stability region for the transverse system is decreasing as the number of moments in the system are increasing. On the other hand, the critical wavenumber profiles for the longitudinal system predicted by various moment theories are quite different from each other, especially for small values of coefficient of restitution ($0 \leq e \lesssim 0.4$). From the left panel of figure 14, it seems that based on the critical wavenumber profiles, one can classify the Grad moment theories into two groups: one containing the G13 and G20 theories and the other containing the G14, G21 and G26 theories. Notice that the first group of theories does not contain the perturbed part of the scalar moment $\tilde{\Delta}$ in contrast to the other group of theories. One can see that the critical wavenumber profiles predicted by the G13 and G20 theories, which do not contain $\tilde{\Delta}$, are very different from those predicted by the G14, G21 and G26 theories, which contain $\tilde{\Delta}$. The critical wavenumber from the G20 theory closely follows that from the G13 theory for $0.25 \lesssim e \leq 1$ and they both have a sudden jump at around $e \approx 0.35$; nevertheless, for $0 \leq e \lesssim 0.21$, the G13 theory does not give any critical wavenumber whereas the G20 theory does give critical wavenumbers, which means that the longitudinal system associated with G13 equations is always unstable for $0 \leq e \lesssim 0.21$ while that associated with G20 equations is stable above a critical wavenumber for all value of e . This also means that the addition of more moments into the system is stabilizing the longitudinal system associated with the G13 equations. In the other group of theories (G14, G21 and G26), the critical wavenumber profiles from the longitudinal system associated with the G14 and G21 are qualitatively similar—including kinks at $e \approx 0.24$ and $e \approx 0.21$ in critical wavenumber profiles for G14 and G21 theories, respectively—since they both contain $\tilde{\Delta}$ and do not contain \hat{R}_{ij} . The instability region for the longitudinal system associated with the G26 equations is also more than that associated with G14 and G21 equations. It may also be stated from the left panel of figure 14 that the number of moments ought to be increased as the inelasticity increases; while stating this, we have ignored the G20 theory (pink curve in the figure) which is, any way, not meaningful for granular gases since it does not contain the scalar fourth order moment.

7. Conclusion

Higher-order Grad's moment equations—up to first 26-moments—for granular gases have been derived by employing the Grad's method of moments to the inelastic Boltzmann equation, and the production terms associated with the derived moment equations have been presented. The production terms have, in fact, been computed and presented for the G27 system (which consists of the first 26-moments and the fully contracted sixth moment). The production terms associated with the G26 equations can easily be computed by dropping the terms containing the fully contracted sixth moment in the given production terms associated with the G27 equations. The HCS of a freely cooling granular gas has been explored with the G26 equations in a semi-linearized setting and it has been found that the temperature decay in the HCS closely follows Haff's law while the other higher-order moments decay on a faster time scale. Further, the nonlinear

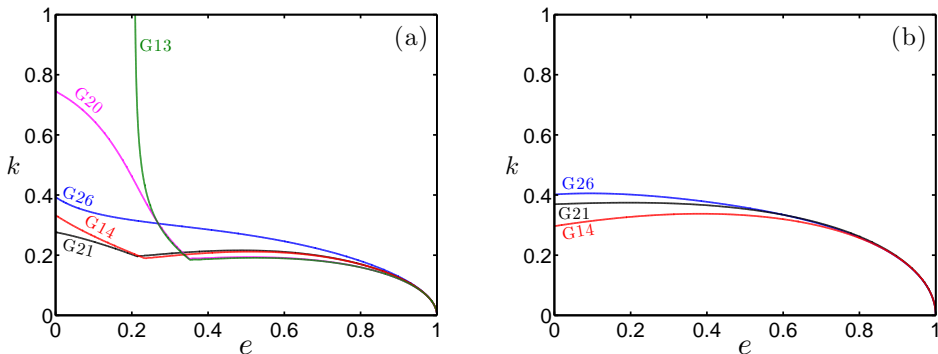


FIGURE 14. Stability diagram in (e, k) -plane for (a) longitudinal and (b) transverse systems associated with various moment theories (G13, G14, G20, G21, G26). The system is unstable below or left of the curves while stable above or right of the curves. The curves from G13 theory are equivalent to those from the theory of [Kremer & Marques Jr. \(2011\)](#).

terms of fully contracted fourth moment have also been included and, by exploiting the stability analysis of fixed points in a dynamical system, it has been shown that some of the fixed points of the system are unstable and with the only stable fixed point it has been concluded that the nonlinear terms, indeed, have only negligible effect on Haff's law. The G27 equations has also been scrutinized and the stability analysis of fixed points in a dynamical system has again been exploited to deduce that even the inclusion of scalar sixth order moment into the G26 system has negligible effect on Haff's law. By performing a Chapman–Enskog-like expansion on the G26 equations, the constitutive relations for the stress and heat flux (the Navier–Stokes and Fourier relations) in five moment theory have been obtained and compared with those in [Kremer & Marques Jr. \(2011\)](#) and with those in [Pekeris & Alterman \(1957\)](#) (for elastic case). The fact that the heat flux in case of an inelastic gas not only depends on the temperature gradient but also on the (number) density gradient has been established with the G26 equations as well. Moreover, as expected, the coefficient of (number) density gradient in the constitutive relation for heat flux vanished in elastic case since it has turned out to be proportional to $(1 - e)$. The transport coefficients in the Navier–Stokes and Fourier relations from G26 theory have turned out to be qualitatively similar to those from the G14 theory of [Kremer & Marques Jr. \(2011\)](#) for large coefficient of restitution ($0.75 \lesssim e \leq 1$) but for small to moderate values of the coefficient of restitution, the transport coefficients from both the theories have differed significantly. The differences were more pronounced for both the transport coefficients in the heat flux (i.e., for the coefficient of thermal conductivity κ and coefficient λ). For molecular gases, the G26 theory gave better value of shear viscosity μ than that from the G14 theory of [Kremer & Marques Jr. \(2011\)](#).

The linear stability of the HCS has been analyzed through the G26 system and various sub-systems by decomposing them into longitudinal and transverse systems. It has been found that one stationary eigenmode in both the longitudinal and transverse systems in case of inelastic gases is unstable whereas all the eigenmodes for both the systems are stable in case of molecular gases. By comparing the eigenmodes from various theories, it has been established that the unstable eigenmode for the longitudinal system obtained with the 13-field eigenmode theory of [Kremer & Marques Jr. \(2011\)](#) remains unstable below a certain coefficient of restitution whereas that obtained with any other higher-order moment theory becomes stable above some critical wavenumber for all values of coefficient of restitution. This is apparently a consequence of assuming the dimensionless

fourth moment as a constant in [Kremer & Marques Jr. \(2011\)](#) rather than considering it as a field variable while analyzing the eigenmodes. Out of all the theories considered, the G26 theory have produced the smoothest critical wavenumber profile. The critical wavenumber profiles from various Grad's moment theories also suggested that the number of moments ought to be increased with increasing inelasticity. Thus, the 14-moment theory of [Kremer & Marques Jr. \(2011\)](#) may not be appropriate for granular gases having large inelasticity (or small coefficient of restitution). On the other hand, the G26 theory seems to be adequate for all granular gases which can be described by assuming a constant coefficient of restitution.

Acknowledgments

PS acknowledges financial support from IIT Madras in the form of New Faculty Initiation Grant (MAT/15-16/833/NFIG/PRIY) and New Faculty Seed Grant (MAT/16-17/671/NFSC/PRIY).

Appendix A. Production terms

The fully nonlinear production terms associated with the G27 equations are given below. The corresponding production terms associated with the G26 equations (eqs. (2.11)–(2.13) and (3.4)–(3.8)) are obtained from (A 1)–(A 6) on taking $\Xi = 0$ and ignoring (A 7).

$$\begin{aligned} \frac{1}{2}\mathcal{P}^1 = & -\frac{5(1-e^2)}{8}\nu\rho\theta\left(1 + \frac{1}{80}\frac{\Delta}{\rho\theta^2} - \frac{1}{6720}\frac{\Xi}{\rho\theta^3} + \frac{1}{25600}\frac{\Delta^2}{\rho^2\theta^4}\right. \\ & + \frac{1}{5160960}\frac{\Xi^2}{\rho^2\theta^6} - \frac{1}{215040}\frac{\Delta\Xi}{\rho^2\theta^5} + \frac{1}{40}\frac{\sigma_{ij}\sigma_{ij}}{\rho^2\theta^2} + \frac{1}{200}\frac{q_iq_i}{\rho^2\theta^3} \\ & \left. + \frac{1}{1680}\frac{m_{ijk}m_{ijk}}{\rho^2\theta^3} + \frac{3}{31360}\frac{R_{ij}R_{ij}}{\rho^2\theta^4} - \frac{1}{560}\frac{\sigma_{ij}R_{ij}}{\rho^2\theta^3}\right), \end{aligned} \quad (\text{A } 1)$$

$$\begin{aligned} \mathcal{P}_{ij}^0 = & -\frac{(1+e)(3-e)}{4}\nu\left[\left(1 - \frac{1}{480}\frac{\Delta}{\rho\theta^2} + \frac{1}{13440}\frac{\Xi}{\rho\theta^3}\right)\sigma_{ij}\right. \\ & + \frac{1}{28}\left(1 + \frac{1}{160}\frac{\Delta}{\rho\theta^2} - \frac{1}{2688}\frac{\Xi}{\rho\theta^3}\right)\frac{R_{ij}}{\theta} + \frac{1}{14}\frac{\sigma_{k\langle i}\sigma_{j\rangle k}}{\rho\theta} + \frac{1}{100}\frac{q_{\langle i}q_{j\rangle}}{\rho\theta^2} \\ & \left. + \frac{1}{504}\frac{m_{kl\langle i}m_{j\rangle kl}}{\rho\theta^2} + \frac{3}{10976}\frac{R_{k\langle i}R_{j\rangle k}}{\rho\theta^3} - \frac{1}{196}\frac{\sigma_{k\langle i}R_{j\rangle k}}{\rho\theta^2} + \frac{1}{140}\frac{m_{ijk}q_k}{\rho\theta^2}\right], \end{aligned} \quad (\text{A } 2)$$

$$\begin{aligned} \frac{1}{2}\mathcal{P}_i^1 = & -\frac{(1+e)}{48}\nu\left[\left\{(49-33e) + \frac{(19-3e)}{480}\frac{\Delta}{\rho\theta^2} - \frac{(53-21e)}{13440}\frac{\Xi}{\rho\theta^3}\right\}q_i\right. \\ & + \frac{3(7+e)}{10}\frac{\sigma_{ij}q_j}{\rho\theta} + \frac{(13-21e)}{280}\frac{R_{ij}q_j}{\rho\theta^2} \\ & \left. + \frac{(11-27e)}{28}\frac{m_{ijk}\sigma_{jk}}{\rho\theta} + \frac{(23+9e)}{784}\frac{m_{ijk}R_{jk}}{\rho\theta^2}\right], \end{aligned} \quad (\text{A } 3)$$

$$\begin{aligned} \mathcal{P}_{ijk}^0 = & -\frac{3(1+e)(3-e)}{8}\nu\left[\left(1 - \frac{1}{1120}\frac{\Delta}{\rho\theta^2} + \frac{1}{94080}\frac{\Xi}{\rho\theta^3}\right)m_{ijk}\right. \\ & \left. - \frac{1}{70}\frac{q_{\langle i}\sigma_{j\rangle k}}{\rho\theta} + \frac{1}{280}\frac{q_{\langle i}R_{j\rangle k}}{\rho\theta^2} + \frac{1}{14}\frac{\sigma_{l\langle i}m_{j\rangle kl}}{\rho\theta} - \frac{1}{1176}\frac{R_{l\langle i}m_{j\rangle kl}}{\rho\theta^2}\right], \end{aligned} \quad (\text{A } 4)$$

$$\begin{aligned}
\mathcal{P}_{ij}^1 = & -\frac{(1+e)}{336}\nu\left[\left\{(499-288e+66e^2-30e^3)+\frac{(137-36e-66e^2+30e^3)}{480}\frac{\Delta}{\rho\theta^2}\right.\right. \\
& -\frac{(215-90e-66e^2+30e^3)}{13440}\frac{\Xi}{\rho\theta^3}\left.\right\}R_{ij}+28\left\{(87-54e+22e^2-10e^3)\right. \\
& -\frac{(55-18e-66e^2+30e^3)}{480}\frac{\Delta}{\rho\theta^2}-\frac{(9+22e^2-10e^3)}{13440}\frac{\Xi}{\rho\theta^3}\left.\right\}\theta\sigma_{ij} \\
& +2(44+27e+66e^2-30e^3)\frac{\sigma_{k\langle i}\sigma_{j\rangle k}}{\rho}+\frac{7(4-15e-66e^2+30e^3)}{25}\frac{q_{\langle i}q_{j\rangle}}{\rho\theta} \\
& +\frac{(28-45e-22e^2+10e^3)}{6}\frac{m_{kl\langle i}m_{j\rangle kl}}{\rho\theta}+\frac{(116-99e-66e^2+30e^3)}{392}\frac{R_{k\langle i}R_{j\rangle k}}{\rho\theta^2} \\
& +\frac{(44+27e+66e^2-30e^3)}{7}\frac{\sigma_{k\langle i}R_{j\rangle k}}{\rho\theta}+\frac{(169-66e^2+30e^3)}{5}\frac{m_{ijk}q_k}{\rho\theta}\left.\right], \quad (\text{A } 5)
\end{aligned}$$

$$\begin{aligned}
\mathcal{P}^2 = & -\frac{5(1+e)}{4}\nu\rho\theta^2\left[(1-e)(9+2e^2)+\frac{(271-207e+30e^2-30e^3)}{240}\frac{\Delta}{\rho\theta^2}\right. \\
& +\frac{(181-117e+10e^2-10e^3)}{6720}\frac{\Xi}{\rho\theta^3}+\frac{(137-9e-30e^2+30e^3)}{230400}\frac{\Delta^2}{\rho^2\theta^4} \\
& +\frac{(91-27e-10e^2+10e^3)}{36126720}\frac{\Xi^2}{\rho^2\theta^6}+\frac{(137-9e-30e^2+30e^3)}{3225600}\frac{\Delta\Xi}{\rho^2\theta^5} \\
& +\frac{(23+9e+30e^2-30e^3)}{120}\frac{\sigma_{ij}\sigma_{ij}}{\rho^2\theta^2}+\frac{(61+3e-30e^2+30e^3)}{600}\frac{q_iq_i}{\rho^2\theta^3} \\
& +\frac{(7-39e-10e^2+10e^3)}{1680}\frac{m_{ijk}m_{ijk}}{\rho^2\theta^3}+\frac{(113-81e-30e^2+30e^3)}{94080}\frac{R_{ij}R_{ij}}{\rho^2\theta^4} \\
& \left.+\frac{(23+9e+30e^2-30e^3)}{1680}\frac{\sigma_{ij}R_{ij}}{\rho^2\theta^3}\right], \quad (\text{A } 6)
\end{aligned}$$

$$\begin{aligned}
\mathcal{P}^3 = & -\frac{15}{16}\nu\rho\theta^3 \left[(115 - 71e^2 - 36e^4 - 8e^6) \right. \\
& + \frac{(8297 + 1408e - 4037e^2 + 512e^3 - 2060e^4 - 280e^6)}{240} \frac{\Delta}{\rho\theta^2} \\
& + \frac{(16841 + 4224e - 7141e^2 + 1536e^3 - 3660e^4 - 280e^6)}{6720} \frac{\Xi}{\rho\theta^3} \\
& - \frac{(551 + 768e + 1301e^2 + 1024e^3 - 340e^4 + 280e^6)}{76800} \frac{\Delta^2}{\rho^2\theta^4} \\
& + \frac{(3113 + 1920e - 3589e^2 - 1536e^3 + 1140e^4 - 280e^6)}{180633600} \frac{\Xi^2}{\rho^2\theta^6} \\
& + \frac{(551 + 768e + 1301e^2 + 1024e^3 - 340e^4 + 280e^6)}{3225600} \frac{\Delta\Xi}{\rho^2\theta^5} \\
& + \frac{(281 + 704e + 939e^2 + 256e^3 + 20e^4 - 280e^6)}{120} \frac{\sigma_{ij}\sigma_{ij}}{\rho^2\theta^2} \\
& + \frac{(685 + 640e + 951e^2 + 1536e^3 - 300e^4 + 840e^6)}{600} \frac{q_i q_i}{\rho^2\theta^3} \\
& + \frac{(95 - 320e - 563e^2 - 768e^3 - 900e^4 + 280e^6)}{1680} \frac{m_{ijk}m_{ijk}}{\rho^2\theta^3} \\
& + \frac{(1641 + 1856e - 581e^2 - 256e^3 + 820e^4 - 280e^6)}{31360} \frac{R_{ij}R_{ij}}{\rho^2\theta^4} \\
& \left. + \frac{(281 + 704e + 939e^2 + 256e^3 + 20e^4 - 280e^6)}{560} \frac{\sigma_{ij}R_{ij}}{\rho^2\theta^3} \right], \tag{A 7}
\end{aligned}$$

where

$$\nu = \frac{16}{5}\sqrt{\pi} n d^2 \sqrt{\theta} \tag{A 8}$$

is the collision frequency.

Appendix B. Governing equations for perturbed field variables

Inserting the field variables from (6.1) into the G26 equations (4.1)–(4.9) and neglecting all the nonlinear terms in perturbations, one obtains the following system of linear partial differential equations in perturbed field variables.

$$\frac{\partial \tilde{n}}{\partial t} + v_H(t) \frac{\partial \tilde{v}_i}{\partial x_i} = 0, \tag{B 1}$$

$$\frac{\partial \tilde{v}_i}{\partial t} + v_H(t) \left[\frac{\partial \tilde{\sigma}_{ij}}{\partial x_j} + \frac{\partial \tilde{n}}{\partial x_i} + \frac{\partial \tilde{T}}{\partial x_i} \right] - \frac{1}{2} \xi_0 \nu_H(t) \tilde{v}_i = 0, \tag{B 2}$$

$$\frac{\partial \tilde{T}}{\partial t} + \frac{2}{3} v_H(t) \left[\frac{\partial \tilde{q}_i}{\partial x_i} + \frac{\partial \tilde{v}_i}{\partial x_i} \left(1 + \frac{\sigma_{ij}^{(H)}(t)}{n_0 T_H(t)} \right) \right] + \nu_H(t) \left[\xi_0 \left(\tilde{n} + \frac{1}{2} \tilde{T} \right) + \frac{(1 - e^2)}{192} \tilde{\Delta} \right] = 0, \tag{B 3}$$

$$\begin{aligned}
& \frac{\partial \tilde{\sigma}_{ij}}{\partial t} + v_H(t) \left[\frac{\partial \tilde{m}_{ijk}}{\partial x_k} + \frac{4}{5} \frac{\partial \tilde{q}_{\langle i}}{\partial x_{j\rangle}} + 2 \frac{\partial \tilde{v}_{\langle i}}{\partial x_{j\rangle}} + \frac{\sigma_{ij}^{(H)}(t)}{n_0 T_H(t)} \frac{\partial \tilde{v}_k}{\partial x_k} + 2 \frac{\sigma_{k\langle i}^{(H)}(t)}{n_0 T_H(t)} \frac{\partial \tilde{v}_{j\rangle}}{\partial x_k} \right] - \xi_0 \nu_H(t) \tilde{\sigma}_{ij} \\
&= -\frac{(1+e)(3-e)}{4} \nu_H(t) \left[\left(1 - \frac{1}{480} \bar{\Delta}_H \right) \left\{ \tilde{\sigma}_{ij} + \frac{\sigma_{ij}^{(H)}(t)}{n_0 T_H(t)} \left(\tilde{n} + \frac{1}{2} \tilde{T} \right) \right\} \right. \\
&\quad + \frac{1}{28} \left(1 + \frac{1}{160} \bar{\Delta}_H \right) \left\{ \tilde{R}_{ij} + \frac{R_{ij}^{(H)}(t)}{n_0 T_H(t) v_H^2(t)} \left(\tilde{n} - \frac{1}{2} \tilde{T} \right) \right\} \\
&\quad \left. + \frac{1}{160} \left(\frac{1}{28} \frac{R_{ij}^{(H)}(t)}{n_0 T_H(t) v_H^2(t)} - \frac{1}{3} \frac{\sigma_{ij}^{(H)}(t)}{n_0 T_H(t)} \right) \tilde{\Delta} \right], \tag{B4}
\end{aligned}$$

$$\begin{aligned}
& \frac{\partial \tilde{q}_i}{\partial t} + v_H(t) \left[\frac{1}{2} \frac{\partial \tilde{R}_{ij}}{\partial x_j} + \frac{1}{6} \frac{\partial \tilde{\Delta}}{\partial x_i} + \frac{1}{6} \bar{\Delta}_H \left(\frac{\partial \tilde{n}}{\partial x_i} + 2 \frac{\partial \tilde{T}}{\partial x_i} \right) + \frac{\partial \tilde{\sigma}_{ij}}{\partial x_j} + \frac{5}{2} \frac{\sigma_{ij}^{(H)}(t)}{n_0 T_H(t)} \frac{\partial \tilde{T}}{\partial x_j} + \frac{5}{2} \frac{\partial \tilde{T}}{\partial x_i} \right. \\
&\quad + \frac{m_{ijk}^{(H)}(t)}{n_0 T_H(t) v_H(t)} \frac{\partial \tilde{v}_j}{\partial x_k} - \frac{\sigma_{ij}^{(H)}(t)}{n_0 T_H(t)} \left(\frac{\partial \tilde{\sigma}_{jk}}{\partial x_k} + \frac{\partial \tilde{n}}{\partial x_j} \right) + \frac{7}{5} \frac{q_i^{(H)}(t)}{n_0 T_H(t) v_H(t)} \frac{\partial \tilde{v}_j}{\partial x_j} \\
&\quad \left. + \frac{q_j^{(H)}(t)}{n_0 T_H(t) v_H(t)} \left(\frac{7}{5} \frac{\partial \tilde{v}_i}{\partial x_j} + \frac{2}{5} \frac{\partial \tilde{v}_j}{\partial x_i} \right) \right] - \frac{3}{2} \xi_0 \nu_H(t) \tilde{q}_i \\
&= -\frac{(1+e)}{48} \nu_H(t) \left[(49 - 33e) + \frac{(19 - 3e)}{480} \bar{\Delta}_H \right] \left[\tilde{q}_i + \frac{q_i^{(H)}(t)}{n_0 T_H(t) v_H(t)} \left(\tilde{n} + \frac{1}{2} \tilde{T} \right) \right] \\
&\quad - \frac{(1+e)}{48} \nu_H(t) \frac{(19 - 3e)}{480} \frac{q_i^{(H)}(t)}{n_0 T_H(t) v_H(t)} \tilde{\Delta}, \tag{B5}
\end{aligned}$$

$$\begin{aligned}
& \frac{\partial \tilde{m}_{ijk}}{\partial t} + v_H(t) \left[\frac{3}{7} \frac{\partial \tilde{R}_{\langle ij}}{\partial x_{k\rangle}} + 3 \frac{\partial \tilde{\sigma}_{\langle ij}}{\partial x_{k\rangle}} - 3 \frac{\sigma_{\langle ij}^{(H)}(t)}{n_0 T_H(t)} \left(\frac{\partial \tilde{\sigma}_{k\rangle l}}{\partial x_l} + \frac{\partial \tilde{n}}{\partial x_{k\rangle}} \right) + \frac{m_{ijk}^{(H)}(t)}{n_0 T_H(t) v_H(t)} \frac{\partial \tilde{v}_l}{\partial x_l} \right. \\
&\quad \left. + 3 \frac{m_{l\langle ij}^{(H)}(t)}{n_0 T_H(t) v_H(t)} \frac{\partial \tilde{v}_{k\rangle}}{\partial x_l} + \frac{12}{5} \frac{q_{\langle i}^{(H)}(t)}{n_0 T_H(t) v_H(t)} \frac{\partial \tilde{v}_j}{\partial x_{k\rangle}} \right] - \frac{3}{2} \xi_0 \nu_H(t) \tilde{m}_{ijk} \\
&= -\frac{3(1+e)(3-e)}{8} \nu_H(t) \left(1 - \frac{1}{1120} \bar{\Delta}_H \right) \left[\tilde{m}_{ijk} + \frac{m_{ijk}^{(H)}(t)}{n_0 T_H(t) v_H(t)} \left(\tilde{n} + \frac{1}{2} \tilde{T} \right) \right] \\
&\quad + \frac{3(1+e)(3-e)}{8} \nu_H(t) \frac{1}{1120} \frac{m_{ijk}^{(H)}(t)}{n_0 T_H(t) v_H(t)} \tilde{\Delta}, \tag{B6}
\end{aligned}$$

$$\begin{aligned}
& \frac{\partial \tilde{R}_{ij}}{\partial t} + v_H(t) \left[\frac{R_{ij}^{(H)}(t)}{n_0 T_H(t) v_H^2(t)} \frac{\partial \tilde{v}_k}{\partial x_k} + \frac{28}{5} \frac{\partial \tilde{q}_{\langle i}}{\partial x_{j\rangle}} + \frac{28}{5} \frac{q_{\langle i}^{(H)}(t)}{n_0 T_H(t) v_H(t)} \frac{\partial \tilde{T}}{\partial x_{j\rangle}} \right. \\
& + 4 \frac{\sigma_{k\langle i}^{(H)}(t)}{n_0 T_H(t)} \left(\frac{\partial \tilde{v}_k}{\partial x_{j\rangle}} + \frac{\partial \tilde{v}_j}{\partial x_k} \right) - \frac{\sigma_{ij}^{(H)}(t)}{n_0 T_H(t)} \left(\frac{8}{3} \frac{\partial \tilde{v}_k}{\partial x_k} + \frac{14}{3} \frac{\partial \tilde{q}_k}{\partial x_k} + \frac{14}{3} \frac{\sigma_{kl}^{(H)}(t)}{n_0 T_H(t)} \frac{\partial \tilde{v}_k}{\partial x_l} \right) \\
& + 2 \frac{\partial \tilde{m}_{ijk}}{\partial x_k} + \frac{6}{7} \frac{R_{\langle ij}^{(H)}(t)}{n_0 T_H(t) v_H^2(t)} \frac{\partial \tilde{v}_k}{\partial x_k} + \frac{R_{k\langle i}^{(H)}(t)}{n_0 T_H(t) v_H^2(t)} \left(\frac{4}{5} \frac{\partial \tilde{v}_k}{\partial x_{j\rangle}} + 2 \frac{\partial \tilde{v}_j}{\partial x_k} \right) \\
& + \frac{14}{15} \bar{\Delta}_H \frac{\partial \tilde{v}_{\langle i}}{\partial x_{j\rangle}} + \frac{m_{ijk}^{(H)}(t)}{n_0 T_H(t) v_H(t)} \left(7 \frac{\partial \tilde{T}}{\partial x_k} - 2 \frac{\partial \tilde{n}}{\partial x_k} - 2 \frac{\partial \tilde{\sigma}_{kl}}{\partial x_l} \right) \\
& \left. - \frac{28}{5} \frac{q_{\langle i}^{(H)}(t)}{n_0 T_H(t) v_H(t)} \left(\frac{\partial \tilde{\sigma}_{j\rangle k}}{\partial x_k} + \frac{\partial \tilde{n}}{\partial x_{j\rangle}} \right) \right] - 2\xi_0 \nu_H(t) \tilde{R}_{ij} \\
& = -\frac{(1+e)}{336} \nu_H(t) \left[\left\{ (436 - 267e + 66e^2 - 30e^3) - \frac{(52 - 27e + 66e^2 - 30e^3)}{480} \bar{\Delta}_H \right\} \right. \\
& \times \left\{ \tilde{R}_{ij} + \frac{R_{ij}^{(H)}(t)}{n_0 T_H(t) v_H^2(t)} \left(\tilde{n} + \frac{1}{2} \tilde{T} \right) \right\} \\
& - 28 \left\{ (11 - 2e - 22e^2 + 10e^3) + \frac{(202 - 207e - 66e^2 + 30e^3)}{480} \bar{\Delta}_H \right\} \\
& \times \left\{ \tilde{\sigma}_{ij} + \frac{\sigma_{ij}^{(H)}(t)}{n_0 T_H(t)} \left(\tilde{n} + \frac{3}{2} \tilde{T} \right) \right\} - \frac{(52 - 27e + 66e^2 - 30e^3)}{480} \frac{R_{ij}^{(H)}(t)}{n_0 T_H(t) v_H^2(t)} \tilde{\Delta} \\
& \left. - 28 \frac{(202 - 207e - 66e^2 + 30e^3)}{480} \frac{\sigma_{ij}^{(H)}(t)}{n_0 T_H(t)} \tilde{\Delta} \right], \tag{B 7}
\end{aligned}$$

$$\begin{aligned}
& \frac{\partial \tilde{\Delta}}{\partial t} + v_H(t) \left[\left(8 - \frac{4}{3} \bar{\Delta}_H \right) \left(\frac{\partial \tilde{q}_i}{\partial x_i} + \frac{\sigma_{ij}^{(H)}(t)}{n_0 T_H(t)} \frac{\partial \tilde{v}_i}{\partial x_j} \right) \right. \\
& \left. - 8 \frac{q_i^{(H)}(t)}{n_0 T_H(t) v_H(t)} \left(\frac{\partial \tilde{\sigma}_{ij}}{\partial x_j} + \frac{\partial \tilde{n}}{\partial x_i} - \frac{5}{2} \frac{\partial \tilde{T}}{\partial x_i} \right) + 4 \frac{R_{ij}^{(H)}(t)}{n_0 T_H(t) v_H^2(t)} \frac{\partial \tilde{v}_i}{\partial x_j} \right] \\
& = -\frac{5(1+e)}{4} \nu_H(t) \left[\frac{(81 - 17e + 30e^2 - 30e^3)}{240} - \frac{(1-e)}{60} \bar{\Delta}_H \right] \tilde{\Delta}, \tag{B 8}
\end{aligned}$$

where

$$\nu_H(t) = \frac{16}{5} \sqrt{\pi} n_0 d^2 \sqrt{\frac{T_H(t)}{m}} \quad \text{and} \quad \xi_0 = \frac{5}{12} (1 - e^2) \left(1 + \frac{1}{80} \bar{\Delta}_H \right).$$

REFERENCES

- ALAM, M., CHIKKADI, V. & GUPTA, V. K. 2009 Density waves and the effect of wall roughness in granular Poiseuille flow: Simulation and linear stability. *Eur. Phys. J. ST* **179**, 69–90.
- BISI, M., SPIGA, G. & TOSCANI, G. 2004 Grad's equations and hydrodynamics for weakly inelastic granular flows. *Phys. Fluids* **16**, 4235–4247.
- BIZON, C., SHATTUCK, M. D., SWIFT, J. B. & SWINNEY, H. L. 1999 Transport coefficients for granular media from molecular dynamics simulations. *Phys. Rev. E* **60**, 4340–4351.

- BOBYLEV, A. V. 1982 The Chapman-Enskog and Grad methods for solving the Boltzmann equation. *Sov. Phys. Dokl.* **27**, 29–31.
- BREU, A. P. J., ENSNER, H.-M., KRUELLE, C. A. & REHBERG, I. 2003 Reversing the Brazil-nut effect: Competition between percolation and condensation. *Phys. Rev. Lett.* **90**, 014302.
- BREY, J. J., DUFTY, J. W., KIM, C. S. & SANTOS, A. 1998 Hydrodynamics for granular flow at low density. *Phys. Rev. E* **58**, 4638–4653.
- BREY, J. J., DUFTY, J. W. & SANTOS, A. 1997 Dissipative dynamics for hard spheres. *J. Stat. Phys.* **87**, 1051–1066.
- BREY, J. J., MORENO, F. & DUFTY, J. W. 1996 Model kinetic equation for low-density granular flow. *Phys. Rev. E* **54**, 445–456.
- BRILLIANTOV, N. V. & PÖSCHEL, T. 2004 *Kinetic Theory of Granular Gases*. New York: Oxford University Press.
- CAMPBELL, C. S. 1990 Rapid granular flows. *Annu. Rev. Fluid Mech.* **22**, 57–90.
- CHAPMAN, S. & COWLING, T. G. 1970 *The Mathematical Theory of Non-Uniform Gases*. Cambridge, UK: Cambridge University Press.
- CORWIN, E. I., JAEGER, H. M. & NAGEL, S. R. 2005 Structural signature of jamming in granular media. *Nature* **435**, 1075–1078.
- GARZÓ, V. 2013 Grad's moment method for a granular fluid at moderate densities: Navier-Stokes transport coefficients. *Phys. Fluids* **25**, 043301.
- GARZÓ, V. & DUFTY, J. W. 1999 Dense fluid transport for inelastic hard spheres. *Phys. Rev. E* **59**, 5895–5911.
- GARZÓ, V. & SANTOS, A. 2003 *Kinetic Theory of Gases in Shear Flows. Nonlinear Transport*. Dordrecht: Kluwer Academic Publishers.
- GOLDHIRSCH, I. 2003 Rapid granular flows. *Annu. Rev. Fluid Mech.* **35**, 267–293.
- GOLDSHTEIN, A. & SHAPIRO, M. 1995 Mechanics of collisional motion of granular materials. part 1. General hydrodynamic equations. *J. Fluid Mech.* **282**, 75–114.
- GRAD, H. 1949*a* Note on N -dimensional Hermite polynomials. *Comm. Pure Appl. Math.* **2**, 325–330.
- GRAD, H. 1949*b* On the kinetic theory of rarefied gases. *Comm. Pure Appl. Math.* **2**, 331–407.
- GUPTA, V. K. 2011 Kinetic theory and Burnett order constitutive relations for a smooth granular gas. Master's thesis, JNCASR, Bangalore, India.
- GUPTA, V. K. 2015 Mathematical modeling of rarefied gas mixtures. PhD thesis, RWTH Aachen University, Germany.
- GUPTA, V. K. & TORRILHON, M. 2012 Automated Boltzmann collision integrals for moment equations. *AIP Conference Proceedings* **1501**, 67–74.
- GUPTA, V. K. & TORRILHON, M. 2015*a* Comparison of relaxation phenomena in binary gas-mixtures of Maxwell molecules and hard spheres. *Comput. Math. Appl.* **70**, 73–88.
- GUPTA, V. K. & TORRILHON, M. 2015*b* Higher order moment equations for rarefied gas mixtures. *Proc. Roy. Soc. A* **471**, 20140754.
- HAFF, P. K. 1983 Grain flow as a fluid-mechanical phenomenon. *J. Fluid Mech.* **134**, 401–430.
- IKENBERRY, E. & TRUESDELL, C. 1956 On the pressures and the flux of energy in a gas according to Maxwell's kinetic theory, I. *J. Ration. Mech. Anal.* **5**, 1–54.
- JENKINS, J. T. & RICHMAN, M. W. 1985*a* Grad's 13-moment system for a dense gas of inelastic spheres. *Arch. Ration. Mech. An.* **87**, 355–377.
- JENKINS, J. T. & RICHMAN, M. W. 1985*b* Kinetic theory for plane flows of a dense gas of identical, rough, inelastic, circular disks. *Phys. Fluids* **28**, 3485–3494.
- JENKINS, J. T. & SAVAGE, S. B. 1983 A theory for the rapid flow of identical, smooth, nearly elastic, spherical particles. *J. Fluid Mech.* **130**, 187–202.
- KHALIL, N., GARZÓ, V. & SANTOS, A. 2014 Hydrodynamic Burnett equations for inelastic Maxwell models of granular gases. *Phys. Rev. E* **89**, 052201.
- KREMER, G. M. & MARQUES JR., W. 2011 Fourteen moment theory for granular gases. *Kinet. Relat. Models* **4**, 317–331.
- KREMER, G. M., SANTOS, A. & GARZÓ, V. 2014 Transport coefficients of a granular gas of inelastic rough hard spheres. *Phys. Rev. E* **90**, 022205.
- KUDROLI, A., WOLPERT, M. & GOLLUB, J. P. 1997 Cluster formation due to collisions in granular material. *Phys. Rev. Lett.* **78**, 1383–1386.

- LISS, E. D., CONWAY, S. L. & GLASSER, B. J. 2002 Density waves in gravity-driven granular flow through a channel. *Phys. Fluids* **14**, 3309–3326.
- LUN, C. K. K., SAVAGE, S. B., JEFFREY, D. J. & CHEPURNIY, N. 1984 Kinetic theories for granular flow: inelastic particles in Couette flow and slightly inelastic particles in a general flowfield. *J. Fluid Mech.* **140**, 223–256.
- LUTSKO, J. F. 2005 Transport properties of dense dissipative hard-sphere fluids for arbitrary energy loss models. *Phys. Rev. E* **72**, 021306.
- MAXWELL, J. C. 1879 On stresses in rarefied gases arising from inequalities of temperature. *Phil. Trans. R. Soc. Lond.* **170**, 231–256.
- MCMANARA, S. 1993 Hydrodynamic modes of a uniform granular medium. *Phys. Fluids A-Fluid* **5**, 3056–3070.
- MELO, F., UMBANHOWAR, P. B. & SWINNEY, H. L. 1995 Hexagons, kinks, and disorder in oscillated granular layers. *Phys. Rev. Lett.* **75**, 3838–3841.
- MUETH, D. M., DEBREGAS, G. F., KARCZMAR, G. S., ENG, P. J., NAGEL, S. R. & JAEGER, H. M. 2000 Signatures of granular microstructure in dense shear flows. *Nature* **406**, 385–389.
- MULLIN, T. 2000 Coarsening of self-organized clusters in binary mixtures of particles. *Phys. Rev. Lett.* **84**, 4741–4744.
- VAN NOIJE, T. P. C. & ERNST, M. H. 1998 Velocity distributions in homogeneous granular fluids: the free and the heated case. *Granular Matter* **1**, 57–64.
- OTTINO, J. M. & KHAKHAR, D. V. 2000 Mixing and segregation of granular materials. *Ann. Rev. Fluid Mech.* **32**, 55–91.
- PEKERIS, C. L. & ALTERMAN, Z. 1957 Solution of the Boltzmann-Hilbert integral equation II. The coefficients of viscosity and heat conduction. *Proc. Natl. Acad. Sci. USA* **43**, 998–1007.
- POULIQUEN, O., DELOUR, J. & SAVAGE, S. B. 1997 Fingering in granular flows. *Nature* **386**, 816–817.
- RAO, K. K. & NOTT, P. R. 2008 *An Introduction to Granular Flow*. New York: Cambridge University Press.
- RISSO, D. & CORDERO, P. 2002 Dynamics of rarefied granular gases. *Phys. Rev. E* **65**, 021304.
- SAHA, S. & ALAM, M. 2014 Non-Newtonian stress, collisional dissipation and heat flux in the shear flow of inelastic disks: a reduction via Grad’s moment method. *J. Fluid Mech.* **757**, 251–296.
- SELA, N. & GOLDBIRSCH, I. 1998 Hydrodynamic equations for rapid flows of smooth inelastic spheres, to Burnett order. *J. Fluid Mech.* **361**, 41–74.
- SELA, N., GOLDBIRSCH, I. & NOSKOWICZ, S. H. 1996 Kinetic theoretical study of a simply sheared twodimensional granular gas to Burnett order. *Phys. Fluids* **8**, 2337–2353.
- SHUKLA, P. & ALAM, M. 2009 Landau-type order parameter equation for shear banding in granular Couette flow. *Phys. Rev. Lett.* **103**, 068001.
- STROGATZ, S. H. 1994 *Nonlinear Dynamics and Chaos*. Reading, Massachusetts: Addison-Wesley Press.
- STRUCHTRUP, H. 2004 Stable transport equations for rarefied gases at high orders in the Knudsen number. *Phys. Fluids* **16**, 3921–3934.
- STRUCHTRUP, H. 2005 *Macroscopic Transport Equations for Rarefied Gas Flows*. Berlin: Springer.
- TORRILHON, M. 2016 Modeling nonequilibrium gas flow based on moment equations. *Annu. Rev. Fluid Mech.* **48**, 429–458.
- UMBANHOWAR, P. B., MELO, F. & SWINNEY, H. L. 1996 Localized excitations in a vertically vibrated granular layer. *Nature* **382**, 793–796.